EFDA–JET–R(08)04

K.D. Lawson, J. Zacks, I.H. Coffey, K.M. Aggarwal, F.P. Keenan
and JET EFDA contributors

Comparison of Modelled C VUV Line Intensity Ratios with Observations of the Emission from the JET Plasma SOL-I

Progress Towards an Integrated Solution for the ITER Baseline Scenario based on High Current and Highly Shaped Plasma Operation at JET

K.D. Lawson[1], J. Zacks[2], I.H. Coffey[2], K.M. Aggarwal[2], F.P. Keenan[2]
and JET EFDA contributors*

[1]*EURATOM/UKAEA Fusion Association, Culham Science Centre, OX14 3DB, UK.*
[2]*Astrophysics Research Center, School of Mathematics and Physics, Queen's University, Belfast, BT7 1NN, Northern Ireland, UK*
** See annex of M.L. Watkins et al, "Overview of JET Results ", (Proc. 21 st IAEA Fusion Energy Conference, Chengdu, China (2006)).*

Comparison of modelled C VUV line intensity ratios with observations of the emission from the JET plasma SOL - I

K D Lawson[1], J Zacks[2], I H Coffey[2], K M Aggarwal[2], F P Keenan[2] & JET-EFDA Contributors*

JET-EFDA, Culham Science Centre, Abingdon, OX14 3DB, UK
[1] *Euratom/UKAEA Fusion Association, Culham Science Centre, Abingdon, OX14 3DB, UK*
[2] *Astrophysics Research Center, School of Mathematics and Physics, Queen's University, Belfast, BT7 1NN, Northern Ireland, UK*

Abstract

An understanding of the radiation emitted by impurities within a plasma is crucial if spectral line intensities are to be used in detailed studies, such as the analysis of impurity transport. The simplest and most direct check that can be made on any measurements of line intensities is to analyse their ratios, this avoiding uncertainties as to the plasma volume emitting the radiation, the absolute sensitivity calibration of the spectrometer and, in some cases, the need for accurate measurements of parameters such as electron density.

A comparison of measured and modelled line intensity ratios can also lead to instrumental sensitivity calibrations and this has been done for the JET VUV SPRED survey spectrometer by Lawson et al. (2008). At short wavelengths, 100Å – 390Å, this was achieved by comparing the measured and modelled spectral line intensity ratios of a number of Na- and Li-like doublets. The agreement between the measurements and the modelled ratios was good, being of the order of the measurement accuracy, ~6%; this resulted in a particularly accurate sensitivity calibration.

At longer wavelengths, 390Å – 1000Å, a similar approach using C line intensity ratios was tried, C being the main low Z intrinsic impurity in JET. However, the agreement between the measured and modelled C ratios was found to be poorer, with discrepancies of up to ~45%. So as to repeat the accuracy of the short wavelength calibration at longer wavelengths and to gain understanding of the interpretation of spectral line intensity measurements from the plasma edge, a detailed study has been made of the C line intensity ratios. The most thorough analysis has been carried out for the CIV ionization stage, the highest temperature and, therefore, innermost ion always found in the Scrape-Off Layer (SOL) of the JET plasma. Comparisons for CIII and CII are also discussed. The observations have been made using a SPRED and a Schwob-Fraenkel spectrometer, which have near-horizontal lines of sight viewing the core and SOL plasmas. In the present study, ohmic, limiter pulses have been considered.

The discrepancies between the measured and modelled C line intensity ratios are described and various explanations have been investigated. Line blending is the commonest reason for disagreements in the VUV and a full application of the collisional-radiative model requires the inclusion of recombination, particularly from charge exchange collisions. The steady state assumption normally used in the collisional-radiative model has been checked and the possibility of the electron energy distribution being non-Maxwellian is being considered. Of these, only the non-Maxwellian distributions allow better agreement to be achieved, although it is not clear at this stage whether the improvement is fortuitous or a valid explanation of the discrepancy. The effect of line-of-sight

integration through plasma regions with steep gradients has been addressed by Zacks (2008) and may provide an explanation of the discrepancy.

1. Introduction

In order to use the passive emission from a plasma for detailed analyses a description of the emitted radiation is required. This is provided by the collisional-radiative model, which enables the population of an excited state to be determined. When combined with the transition probability of spontaneous radiative decay, the intensity of the line emission due to the transition is obtained. The use of intensity ratios of lines emitted by the same ionization stage avoids the need to determine parameters such as the emitting plasma volume, increasing the reliability of the resulting measurements.

If the model contains all relevant processes, there should be agreement with measurements to within the measurement accuracy. This was indeed found for a number of Na- and Li-like line intensity ratios used to determine the short wavelength (100Å – 390Å) sensitivity calibration of the JET VUV SPRED survey spectrometer (Lawson *et al*., 2008). Only one of the Na- and Li-like line pairs occurs to longer wavelengths in the SPRED spectrum, the NeVIII doublet at 770.4Å and 780.3Å, and, hence, for the long wavelength region of the spectrum an alternative is required. C is the main low Z intrinsic impurity in the JET plasma, many of the plasma facing surfaces being manufactured from Carbon Fibre Composite (CFC) tiles, and a number of C lines occur throughout the VUV spectrum. Consequently, C line intensity ratios were used to extend the sensitivity calibration to longer wavelengths. However, discrepancies between the measured and modelled C line intensity ratios, ~45%, were found, significantly greater than the experimental accuracy of ~6-8%.

In order to explain these discrepancies, a detailed study has been made of the emission from the low ionisation stages of C, CII to CIV, the most thorough being for the Li-like ionization stage, CIV. These ionization stages are found in the Scrape-Off Layer (SOL) of the JET plasma. Since the collisional-radiative model forms the basis of any interpretation of the spectral line emission, whether in the determination of impurity concentrations or for input to transport codes, etc., it was not only hoped to improve the accuracy of the long wavelength SPRED sensitivity calibration, but also to provide a check on the collisional-radiative model and the associated atomic data, outside the environment of the highly complicated impurity transport simulation codes.

The experimental arrangement is described in section 2. Section 3 gives details of the collisional-radiative model and section 4 the comparison between the modelled and observed line intensity ratios. Although as yet, no convincing explanation for the observed discrepancies has been found, a number of possible causes have been investigated and these are discussed in section 5. Further work and conclusions are presented in section 6.

2. Experimental Arrangement

a. Spectrometers

The measurements of the spectral line intensity ratios were made on two instruments, a VUV SPRED spectrometer (Fonck *et al*. 1982) and a Schwob-Fraenkel duo-multichannel spectrometer (Schwob *et al*. 1987). The SPRED instrument is positioned beyond the JET containment wall viewing

the plasma along a radial line of sight in the vessel midplane, a distance of 22m from the plasma. A mirror placed in the beamline focusses the plasma radiation onto the spectrometer entrance slit. This arrangement minimizes neutron noise, allowing the instrument to be used during T campaigns (Coffey *et al*. 2004).

The SPRED spectrometer uses a toroidal, holographic grating to give an intense first order spectrum and a weaker third order spectrum on a flat focal field, the even orders being suppressed. Over its years of use, there has been some degradation of the grating in the JET instrument and the second order can now be seen. On JET, a 450g.mm^{-1} grating is routinely employed resulting in a spectral coverage of 100 to 1100Å. The detector consists of a CuI coated micro-channel plate (MCP) - phosphor combination. The radiation from the phosphor is channelled along optical fibres onto a PhotoDiode Array (PDA). During the period when the analysed data were recorded, the PDA had 1024 pixels available. The instrument's spectral resolution with an extended plasma source is ~5Å and so the FWHM of a spectral line covered ~5 pixels.

The Schwob-Fraenkel spectrometer was situated close to the JET machine, the entrance slit being 5m from the plasma, and has a near-horizontal line of sight. It has a higher spectral resolution than the SPRED instrument, employing a 2m grazing incidence mount. However, this is achieved at the expense of wavelength coverage. With the routinely used 600g.mm^{-1} grating, wavelengths from ~12 to 340Å can be observed by 2 detectors, which can be independently moved around the Rowland circle. The spectral range and resolution of each detector depends on wavelength and varies from 20 to 70Å and from 0.25 to 0.35Å, respectively. The detectors are similar to that of the SPRED, except that a MgF_2 coating is used on the MCPs to enhance the sensitivity at short wavelengths.

b. Plasma configuration

Although now of less interest for plasma physics experiments, the higher intensity of the plasma edge emission observed along a horizontal line of sight during the limiter phase of a discharge makes this the preferred configuration for this study. The blending of the C lines is also minimized, since C is usually the dominant impurity during this phase. A further advantage is that, during a day of operations, the limiter phase of the discharge is usually repeated without alteration a number of times. This allowed the reproducibility of the measurements to be checked, typically a series of 6 pulses being analysed so as to obtain one line intensity ratio.

c. Measurements

The holographic grating of the SPRED spectrometer is designed so that the spectral line profile is the same throughout the spectrum. This leads to a simple and reliable means of integrating the lines by applying Simpson's rule to an area defined by a certain number of pixels on either side of the line centre, these pixels also defining the background to be subtracted. An integration over ±3 pixels from the line centre was used, this range being a compromise between minimizing the blending that occurs because of the instrument's limited spectral resolution and including a sufficient proportion of the line profile to give a reliable measurement. This method also avoids the problem of uncertainties over the choice of the background to be subtracted, which can lead to very significant errors (Lawson *et al*., 1987). Difficulties over the choice of the background can affect the reliability of the integration of both closely packed and weak lines. Generally, this method is preferred to line profile fitting, which is only carried out for a few special cases. This is because the limited number of pixels within a line

requires the fit to be carefully tailored to the particular line being considered so as to ensure reliable results, always a very time consuming procedure; indeed, comparisons of the time histories of the intensities of most lines that are unaffected by blending show no significant discrepancies between the intensities determined from the line being fitted and the area being calculated using the Simpson's rule method. Particular cases where line fitting have been used are discussed later. Comparing the identical limiter phases of series of pulses shows that a measurement reproducibility of <2% was achieved for ratios of lines observed with the SPRED spectrometer.

In order to assess the accuracy of the SPRED measurement of the line intensity, it is also necessary to take into account occasional pixel shifts in the spectrum, which lead to small, but significant variations in the line profiles. These pixel shifts result from the limited mechanical stability of the SPRED spectrometer. The small number of pixels in a line (FWHM ~5 pixels) means that the pixel shifts do affect the measurement. Analyzing the results of line intensity ratios observed over a period of 2 years, during which there were a number of small pixel shifts, shows that an accuracy of better than ~6% can be achieved for the measurement of a line intensity ratio when the lines are isolated and are of moderate to high intensity, that is with a peak intensity in the line profile of $\geq 1.7 \times 10^5$cts.s^{-1}.

In contrast to the line profiles observed on the SPRED instrument, the profiles of the lines observed with the Schwob-Fraenkel spectrometer vary throughout the spectrum. Nevertheless, a similar approach to that used for the SPRED instrument is employed in which the integration is carried out over a fixed number of pixels (Coffey *et al*. 2009). Again, this method is found to be of particular value in dealing with weak lines, of importance in the use of the Schwob-Fraenkel spectrometer in the present study; for example, the 296.9Å line has a typical peak intensity of only 300–450cts.s^{-1}. The accuracy that can be achieved for such lines is estimated from the measurement reproducibility to be ~8%.

The measurements of the line intensity ratios are derived from matching the two line intensities throughout a period of between 4 and 9s during the limiter phase of a pulse when the C intensities were high. In most cases, measurements of 6 pulses with identical limiter phases were averaged to improve the accuracy and reliability of the measurement and to allow a check on the reproducibility to be made. However, in a few instances, particularly those involving the Schwob-Fraenkel measurements, for which the data were more limited, fewer pulses were averaged and it was necessary to use a more limited period within the limiter phase for the comparison. Over 300 pulses were analyzed, 293 being used in the final database.

3. The collisional-radiative model

The calculation of the spectral line intensity of a transition from state i to j,

$$I_{ij} = n_i A_{ij} \quad \text{photons.s}^{-1},$$

requires knowledge of both the Einstein spontaneous emission transition probability, A_{ij}, and of the excited level population, n_i. In the simplest statement of the collisional-radiative model omitting source terms such as ionization and recombination, n_i is determined from the rate equations in which the level i is populated both by collisional excitation and de-excitation and by radiative decay, the positive terms in equation (1), these same processes also resulting in depopulation of level i, which gives rise to the negative terms in the equation,

$$\frac{dn_i}{dt} = n_e \sum_{j \neq i} n_j q_{ji} - n_e \sum_{j \neq i} n_i q_{ij} + \sum_{j>i} n_j A_{ji} - \sum_{j<i} n_i A_{ij}. \quad (1)$$

q_{ij} is the collisional excitation or de-excitation rate from level i to j. In the steady state approximation,

$$\frac{dn_i}{dt} = 0,$$

this leading to a set of simultaneous equations, which can be solved for n_i / n_g, where n_g is the ground level population. Hence, in addition to the transition probabilities, collisional excitation and de-excitation rates are required. For ions such as CII to CIV, the main populating mechanism is electron collisions.

For the CIV ionization stage, Aggarwal and Keenan (2004) provide new transition probabilities and R-matrix calculations of the electron collision strengths, the latter for a wide range of energies. In addition, the R-matrix calculations of Griffin *et al*. (2000) were also used in the comparison. For the other ionization stages, data are taken from the ADAS database (Summers, 2004). For CII the collision strengths reviewed by Sampson *et al*. (1994) are included in the database and for CIII the transition probabilities reviewed by Allard *et al*. (1990), particularly those of Nussbaumer and Storey (1978), and the collision data recommended in a review by Berrington (1994) are used.

Other significant populating mechanisms can be charge exchange with background or injected neutrals and recombination to excited levels. These processes are discussed further in section 5d.

4. Comparisons of observations with modelled line intensity ratios

a. Li-like ionization stage - CIV

i) CIV lines included in the analysis

The innermost of the C ionization stages always occurring in the SOL of the JET plasma is the Li-like stage. Four CIV lines are routinely observed by the SPRED spectrometer at 289.2Å (2p-4d), 312.4Å (2s-3p), 384.1Å (2p-3d) and 419.6Å (2p-3s). With the normally used 450g.mm^{-1} grating, it is not possible to see the CIV lines at 1548.2Å and 1550.8Å (2s-2p). An example of the SPRED spectrum averaged between 4 and 10s for pulse 63445 is shown in figure 1.

In the SPRED spectrum, the 384.1Å line is blended with a number of CIII lines, those at 385.0Å, 386.2Å and 389.0Å being of most concern. The spectrum is best seen with the higher resolution Schwob-Fraenkel spectrometer as shown for pulse 52597 averaged between times 4 and 10s in figure 2; this spectrum is recorded with the occasionally used 300g.mm^{-1} grating. It is evident that the 385.0Å line and the three CIII lines at 389.0Å are weak. Given their intensities, the 389.0Å lines are far enough from the 384.1Å line centre for them to be neglected in the SPRED spectrum. The importance of the 385.0Å line has been checked by modelling the theoretical 538.2Å/385.0Å line intensity ratio and comparing it with the measured 538.2Å/384.1Å ratio. The worst case found was of the intensity of the 385.0Å line being 0.35% of the CIV 384.1Å intensity. Hence, even allowing for significant errors in the model and SPRED sensitivity calibration, the 385.0Å line is small enough to

be neglected. The contribution of the other significant CIII line at 386.2Å to the 384Å line recorded by the SPRED must be removed by line fitting.

The profile of lines observed with the SPRED instrument is dominated by the instrument function and has significant line wings. It is best described by a modified Lorentzian function (Lawson and Peacock, 1988). In making the fits, various analytic functions of this form were tested, but in all cases the height of the 386.2Å line, known in a few cases from the corresponding Schwob-Fraenkel spectra, was seriously overestimated. In the end, another CIII singlet line at 574.3Å was used to fix the height of the 386.2Å line, their ratio being found empirically. A double Gaussian fit was then found to be adequate to describe the central region of the 384Å line and the correction to the line integral when removing the 386.2Å component was found to be small, ~3-9%. Although the 386.2Å/574.3Å ratio is expected to be relatively insensitive to plasma conditions, a check was nevertheless made to determine the sensitivity of the correction to errors in this ratio. It was found that varying the height of the 386.2Å line by a factor of 2 led to a change of at most 7% in the fitted 384.1Å line intensity.

A second CIV line affected by blending in the SPRED spectrum is the 289.2Å line, which in some spectra is blended with the NiXVIII, 292.0Å transition. Two checks can be made to assess the seriousness of this blend. Firstly, another NiXVIII line at 320.6Å, which has ~0.5 the intensity of the 292.0Å line, can be used to monitor the Ni line. It is found that, in comparison to the C lines, the NiXVIII lines are usually weak during the limiter phase of the discharge. Secondly, a comparison has been made between the measurements of the 312.4Å/289.2Å ratio observed with the SPRED and Schwob-Fraenkel spectrometers. With the latter, the 292.0Å line is well separated from the 289.2Å line. In a database of 17 series of pulses, the mean difference in the ratio observed with the two spectrometers was 2.9%, with all but three comparisons agreeing to within 4.5%.

For some pulses, it was also possible to supplement the SPRED observations with measurements of the CIV 244.9Å (2s-4p) and 296.9Å (2p-4s) lines recorded by the Schwob-Fraenkel instrument. The detector position used for the 296.9Å line included observation of the 289.2Å and 312.4Å lines, but no other CIV lines were observed at the same time. The shorter wavelength 244.9Å line was only observed with the 289.2Å line. Figure 3 shows an example of the Schwob-Fraenkel spectrum recorded between times 5 and 12s for pulse 58259. All the CIV lines used in this study, together with their identifications, are listed in table 1.

Table 1. CIV lines used in analysis.

Wavelength (Å)	Transition	Spectrometer used for observation	Blends
244.9	$1s^2 2s\ ^2S_{1/2} - 1s^2 4p\ ^2P_{1/2,3/2}$	S-F	
289.2	$1s^2 2p\ ^2P_{1/2,3/2} - 1s^2 4d\ ^2D_{3/2,5/2}$	S-F / SPRED	NiXVIII, 292.0Å
296.9	$1s^2 2p\ ^2P_{1/2,3/2} - 1s^2 4s\ ^2S_{1/2}$	S-F	
312.4	$1s^2 2s\ ^2S_{1/2} - 1s^2 3p\ ^2P_{1/2,3/2}$	S-F / SPRED	
384.1	$1s^2 2p\ ^2P_{1/2,3/2} - 1s^2 3d\ ^2D_{3/2,5/2}$	SPRED	CIII, 386.2Å
419.6	$1s^2 2p\ ^2P_{1/2,3/2} - 1s^2 3s\ ^2S_{1/2}$	SPRED	

S-F denotes the Schwob-Fraenkel spectrometer.
Line blends are discussed further in section 5b.

ii) Extension of the SPRED sensitivity calibration to 420Å

The availability of a sensitivity calibration for the SPRED instrument at wavelengths below 390Å (Lawson *et al*. 2008) is particularly useful in the present analysis. It was intended to extend this calibration to longer wavelengths using the C line intensity ratios. At the low densities of the SOL, $\leq 10^{19} m^{-3}$, the CIV line intensity ratios are relatively insensitive to n_e, varying by no more than 2.5%. However, they are sensitive to a lesser or greater extent to T_e through the collisional excitation rates, which depend on the particle impact energies. The T_e of the CIV emission region can be determined from the 312.4Å/289.2Å (2s-3p)/(2p-4d) line ratio, for which the sensitivity calibration is known, and then used to predict line intensities ratios for the other CIV transitions. Comparisons with the measured values should allow the sensitivity calibration to be extended up to a wavelength of 420Å.

The 384.1Å/312.4Å (2p-3d)/(2s-3p) line ratio is expected to be much less sensitive to T_e, by a factor of ~6-7, than is found for the 312.4Å/289.2Å line ratio and therefore ideal for checking the sensitivity at 384Å. Nevertheless, the result is found to be inconsistent with the existing calibration. This is determined using intensity ratios for a number of Na- and Li-like doublets, at the higher wavelengths those of Ni XVIII, Fe XVI and Ar XVI being used. This would suggest an inverse sensitivity, S^{-1}, at 384.1Å relative to 312.4Å of 1.33, whereas the value found from the CIV ratio is 1.88, ~40% higher.

The sensitivity at 420Å is calculated using the 312.4Å/419.6Å (2s-3p)/(2p-3s) line intensity ratio. This ratio is also expected to be less temperature dependent, by a factor of ~3-4, than the 312.4Å/289.2Å ratio and, hence, should give a reliable calibration. In fact, correcting for T_e, rather than significantly reducing the scatter in the results, marginally increases the scatter. Further, there is a clear T_e dependence in the derived 'inverse sensitivity', as is shown in figure 4. An average value of S^{-1} relative to 312.4Å is 3.21.

iii) Time behaviour of the 289Å, 312Å and 420Å lines

Since the 312.4Å/419.6Å line intensity ratio is expected to have a smaller temperature sensitivity than the 312.4Å/289.2Å ratio, the time histories of the 312.4Å (2s-3p) and 419.6Å (2p-3s) lines are expected to follow each other more closely than those of the 289.2Å (2p-4d) and 312.4Å lines. However, a number of pulses are found in which it is the 419.6Å line whose time history deviates from the others. Those of the 289.2Å and 312.4Å lines usually follow one another closely. An example is shown in figure 5; in pulse 56907, the 419.6Å line intensity increases to become ~20% higher than the 289.2Å and 312.4Å line intensities. About 17% of the pulses analysed clearly showed such a behaviour, whereas less than 1% of pulses were found in which the 289.2Å line deviated from the other two. Generally the 419.6Å line intensity increased relative to the 289.2Å and 312.4Å intensities, although a few pulses with the opposite behaviour (~1.7%) were found.

iv) Measurement of electron temperature

A crucial test of the collisional-radiative model is whether it gives a consistent electron temperature for the plasma region in which the radiating ions are located. An accurate sensitivity calibration is available for lines forming three line intensity ratios. The 312.4Å/289.2Å (2s-3p)/(2p-4d) ratio observed on the SPRED has a particularly reliable calibration. In addition, a calibration is available for the 289.2Å/244.9Å (2p-4d)/(2s-4p) and 312.4Å/296.9Å (2s-3p)/(2p-4s) ratios observed with the Schwob-Fraenkel spectrometer. Figures 6 and 7 plot the electron temperatures derived from these ratios using the atomic data of Aggarwal and Keenan (2004). Figures 6a and 7a directly

compare the temperatures from, respectively, the 289.2Å/244.9Å and 312.4Å/296.9Å ratios with that from the 312.4Å/289.2Å ratio. Figures 6b and 7b plot the ratio of the temperatures, which clearly should be 1, against the 312.4Å/289.2Å temperature. The 312.4Å/296.9Å ratio suggests an electron temperature in the range 9.8 to 11eV, which is similar to that found from the 312.4Å/289.2Å ratio, 11 to 15eV. However, the 289.2Å/244.9Å ratio gives a temperature significantly lower, 1.5 to 4.2eV. In neither case are ratios of the temperatures constant.

There is also a sensitivity calibration for the 384.1Å (2p-3d) line observed with the SPRED spectrometer, although this may be somewhat less accurate (~ ±15%) than the sensitivities at 289.2Å and 312.4Å (< ±10%) and as already noted in section 4a ii) it differs significantly from the sensitivity derived from the CIV line ratios. Figures 8 to 11 illustrate comparisons of temperatures derived from other line ratios involving, in addition, the 384.1Å and 419.6Å (2p-3s) lines. For the latter, the sensitivity calibration as given by Lawson *et al*. (2008) has been used. Differences in the derived temperatures may in part be due to uncertainties in the sensitivity calibrations for these lines.

In order to describe the trends seen in figures 6 to 11, a parameter denoting the discrepancy is defined as

$$d(T_e) = \frac{R_m}{R_t}, \tag{2}$$

where R_m is the measured intensity ratio and R_t is the theoretical ratio modelled at the temperature derived from the 312.4Å/289.2Å (2s-3p)/(2p-4d) line ratio. The latter ratio is chosen, because the sensitivity calibration at these wavelengths is particularly reliable. Straight line fits are carried out to the discrepancies for the ratios 419.6Å/312.4Å (2p-3s)/(2s-3p), 419.6Å/289.2Å (2p-3s)/(2p-4d), 384.1Å/312.4Å (2p-3d)/(2s-3p), 296.9Å/312.4Å (2p-4s)/(2s-3p) and 244.9Å/312.4Å (2s-4p)/(2s-3p) as a function of T_e, these being shown in figures 12 to 16. In making the fits only points clearly following the main trend are used, extreme points being excluded. In figures 12 and 13, it can be seen that plotting the 419.6Å (2p-3s) line as a ratio with either the 312.4Å (2s-3p) or 289.2Å (2p-4d) line makes little difference and this is the case for the other lines. In figure 15 a very well-defined trend is seen and this is thought due to the majority of the 296.9Å (2p-4s) data being recorded with nearly the same spectrometer detector positions (77% of pulses with 384 and 385mm and 86% with 380, 384 and 385mm). Table 2 lists the fit parameters defining the straight lines and the standard errors in the gradients. In all cases, the standard errors are smaller than the gradients confirming the temperature dependence of the discrepancies. It is also clear that the 419.6Å (2p-3s) line and to a lesser extent the 244.9Å (2s-4p) lines are exceptional, in that they have a strong temperature dependence.

Table 2. Fit parameters to the discrepancies in the line intensity ratios.

Ratio	Gradient	Constant term	Standard error in the gradient
419.6Å/312.4Å	0.0693	-0.1750	0.0049
419.6Å/289.2Å	0.0710	-0.1966	0.0049
384.1Å/312.4Å	-0.0292	1.0823	0.0028
296.9Å/312.4Å	-0.0156	1.0473	0.0025
244.9Å/312.4Å	0.0423	0.6505	0.0087

From the fits, 'measured' ratios have been recalculated and from these the corresponding temperatures determined to those displayed in figures 6 to 11. These recalculated temperatures are

shown as lines in these diagrams and it can be seen that they satisfactorily describe the trends in the data. It is noted that the atomic data of Griffin *et al*. (2000) shifted the discrepancies to higher temperatures, but with little change to the shape of the fits.

b. Be-like ionization stage - CIII

i) CIII lines included in the analysis

A number of CIII lines occur throughout the SPRED spectrum, making this ionization stage of particular interest with regard to the spectrometer calibration. However, some of the lines are blended and others are weak. Table 3 lists those lines used in the present study. All the lines are at wavelengths above 340Å and so were recorded by the SPRED spectrometer. It can be seen that the shorter wavelength lines belong to the triplet spin system and the two longest wavelength lines to singlet transitions. Only ratios of lines within the same spin system were used, so as to avoid uncertainties due to a metastable population in the 2s2p ^{3}P levels.

Table 3. CIII lines used in analysis.

Wavelength (Å)	Transition	Blends
341.2	$2s2p\ ^3P_{0,1,2} - 2s5d\ ^3D_{1,2,3}$	
369.4	$2s2p\ ^3P_{0,1,2} - 2p3p\ ^3D_{1,2,3}$	CIII, 371.7Å
371.7	$2s2p\ ^3P_{0,1,2} - 2s4d\ ^3D_{1,2,3}$	CIII, 369.4Å
459.6	$2s2p\ ^3P_{0,1,2} - 2s3d\ ^3D_{1,2,3}$	
538.2	$2s2p\ ^3P_{0,1,2} - 2s3s\ ^3S_1$	
574.3	$2s2p\ ^1P_1 - 2s3d\ ^1D_2$	
977.0	$2s^2\ ^1S_0 - 2s2p\ ^1P_1$	

Of the CIII lines not included, those at 385.0Å, 386.2Å and 389.0Å are blended with the CIV, 384.1Å line, this blend being dealt with in section 4a. There was also concern about the blending of the 459.6Å and 538.2Å lines with, respectively, the weaker 460.0Å and 535.3Å singlet lines. By comparing measurements of the 977.0Å/459.6Å and 977.0Å/538.2Å line intensity ratios with predicted ratios of the singlet 460.0Å, 535.3Å and 977.0Å transitions, the importance of the 460.0Å and 535.3Å transitions was estimated. The 460.0Å line intensity was found to be less than 0.1% of that of the 459.6Å line and the 535.3Å intensity at most 0.3% of the intensity of the 538.2Å line as well as being offset from the line centre. Even allowing for uncertainties in the theory and the spectrometer's sensitivity calibration, these estimates suggest that the 460.0Å and 535.3Å lines can be neglected. Finally, it is noted that the CIII, 585.5Å line is thought unreliable, because it is blended with both HeI at 584.3Å and, if present, ArVII at 585.8Å.

In the SPRED spectrum, the two triplet lines at wavelengths of 369.4Å and 371.7Å are blended and so a double Gaussian fit was carried out to obtain a reliable measurement of the total intensity of the blended line. It was found necessary to fix the relative intensities of the two components. Theoretically, the 369.4Å/371.7Å line intensity ratio is ~0.4 and this is consistent with the observation of these lines in the more highly resolved Schwob-Fraenkel spectrum recorded with the 300g.mm^{-1} grating. An example is shown in figure 2, in which a ratio of 0.43 is measured. A check was made to

determine the sensitivity of the final result to the line intensity ratio used in the fit and it was found that varying the ratio from 0.3 to 0.5 results in less than 5% variation in the total line intensity. Hence, using a single pre-defined 369.4Å/371.7Å ratio for all pulses should not introduce significant errors.

ii) Consistency of CIII data

As in the case of CIV, the shortest wavelength CIII lines fall in the spectral region for which there is an independent sensitivity calibration for the SPRED spectrometer. These are the triplet CIII line at 341.2Å (2s2p-2s5d) and the blend of the 369.4Å (2s2p-2p3p) and 371.7Å (2s2p-2s4d) lines. Although the (369.4Å+371.7Å)/341.2Å ratio is not especially temperature sensitive and therefore not useful for determining T_e, it does provide a check on the model for CIII. Theoretical ratios are listed in table 4 and measured ratios for a number of pulse ranges in table 5. It is noted that the results from the model for these and the other CIII ratios discussed are not dependent on electron density in the range 10^{17} – $10^{19}m^{-3}$. Between wavelengths of 360.8Å and 389.1Å there is a fall in the spectrometer sensitivity, this resulting in a poorer accuracy for the 371Å sensitivity than at shorter wavelengths. The accuracy of the sensitivity is nevertheless estimated to be –9%/+13%. Even allowing for such errors, the measurements of the ratios are lower than expected theoretically for all but the highest T_e. These are similar to the CIII ionization potential (48eV) and are higher than would be expected for this ionization stage. The CIII temperature is estimated to be ~7–10eV. This is derived by making comparisons with the T_e measured for CIV using the 312.4Å/289.2Å ratio and the ionization potentials (64eV for CIV) and the temperatures of maximum abundance under ionization equilibrium (4eV for CIII and 7.5eV for CIV). For the estimated temperatures of 7-10eV, the measurements of the (371.7Å+369.4Å)/341.2Å ratio are 30 – 40% lower than expected from the model. It is noted that a check for blends with these lines has been carried out, but with no obvious candidates being found.

Table 4. Modelled values of the (371.7Å+369.4Å)/341.2Å line intensity ratio.

T_e	371.7Å/341.2Å ratio	369.4Å/341.2Å ratio	(371.7Å+369.4Å)/341.2Å ratio
5	4.31	1.61	5.92
6	3.90	1.49	5.39
7	3.64	1.41	5.05
8	3.45	1.35	4.80
9	3.32	1.31	4.63
10	3.21	1.28	4.49
12	3.06	1.23	4.29
15	2.91	1.19	4.10
20	2.76	1.16	3.92
30	2.61	1.13	3.74
50	2.49	1.14	3.63

The pulse ranges listed in table 5 were chosen so as to give a wide range of conditions, as indicated by the CIV temperature derived from the 312.4Å/289.2Å ratio, it being supposed that a high CIV T_e will correspond to a high CIII T_e and vica versa. In fact, this correspondence appears to be weak. There were a series of small pixel shifts in the SPRED spectrum over the period in which data

were recorded, leading to slightly differing spectral line profiles. Comparisons for pulse ranges that have lines with the same profile, denoted by the letter in the first column of table 5, are accurate to the reproducibility of the measurement, better than 2%. For the pulse ranges with profile A, the CIII measurements suggest the opposite ordering of the temperatures than would be expected from the CIV T_e.

Table 5. Measurements of the (371.7Å+369.4Å)/341.2Å line intensity ratio.

Spectral line profile	Pulse range	Measured (371.7Å+369.4Å)/341.2Å ratio	T_e for CIV from 312.4Å/289.2Å ratio
A	56016 – 56021	3.04	11.4
A	56138 – 56144	3.13	12.2
B	58799 – 58805	3.06	12.0
C	59096 – 59102	3.12	13.5
D	59210 – 59215	3.02	12.5
E	61518 – 61520	3.24	14.0
E	63367 - 63372	3.20	13.1

The C line intensity ratios have been used to derive the sensitivity calibration for the long wavelength region of the SPRED spectrum as described by Lawson *et al*. (2008). However the accuracy of the derived calibration, estimated to be ~ ±45%, is poorer than at shorter wavelengths and is limited by the uncertainties in the application of the collisional-radiative model.

c. B-like ionization stage - CII

i) CII lines included in the analysis

Only three useful CII lines have been found and one of these at 687.2Å is blended with the CIII line at 690.5Å. The intensity of the 690.5Å line was estimated in the same way as for the 460.0Å and 535.3Å CIII lines. In this case, however, it was clear that the contribution of the 690.5Å line could be significant. Nevertheless, it is noted that where differences in the time histories of intense CII and CIII lines are seen, such as for the 904.1Å and 977.0Å lines, the 687.2Å time history follows that of the CII line, rather than of the CIII line. Such differences could be seen most clearly in the first few seconds of the pulse. Table 6 lists the CII transitions used in the study. The long wavelengths of the CII lines means that all their observations were made using the SPRED spectrometer.

Table 6. CII lines used in analysis.

Wavelength (Å)	Transition	Blends
594.9	$2s^2 2p\ ^2P_{1/2,3/2} - 2s^2 4d\ ^2D_{3/2,5/2}$	
687.2	$2s^2 2p\ ^2P_{1/2,3/2} - 2s^2 3d\ ^2D_{3/2,5/2}$	CIII, 690.5Å
904.1	$2s^2 2p\ ^2P_{1/2,3/2} - 2s2p^2\ ^2P_{1/2,3/2}$	

ii) Consistency of CII data

The line intensity ratios within the CII ionization stage have some density sensitivity for electron densities above $10^{18}m^{-3}$ and are strongly dependent on temperature. The temperature of the CII emitting region is estimated in the same way as for CIII to be ~3.2–4.7eV. Comparisons of the measurements with the modelled results were used in deriving the long wavelength sensitivity calibration for the SPRED instrument, although with greater uncertainty than that derived for the short wavelengths (Lawson *et al*. 2008). It is noted that in comparing the measured and modelled data, there is no indication that the 687.2Å line is seriously blended, although the range of the possible modelled results is wide.

5. Discussion

a. Measurement accuracies

In comparing modelled and experimental results, the expectation is that the limiting factor will be the accuracy of the measurements. As discussed in section 2c, line ratios measured on the SPRED spectrometer with a peak line intensity of $\geq 1.7 \times 10^{5} cts.s^{-1}$, which includes all the CIV lines measured by this instrument used in the present study, generally have an accuracy of better than ~6%. In the case of the Schwob-Fraenkel spectrometer, which has been used to measure weak lines, the accuracy is somewhat poorer being typically ~8%; this can be seen in the wider spread in the measurements when averaging similar pulses. In figures 12 to 16, the spread of the measurements about the straight line fits are consistent with the above accuracies. It is also clear from these diagrams that the observed discrepancies are significantly larger than the measurement errors.

This contrasts with the good agreement found between the measured and modelled results of the Na- and Li-like metal line intensity ratios, used to derive the short wavelength SPRED sensitivity calibration, for which the only limitation found was the accuracy to which the line intensities could be measured (Lawson *et al*., 2008).

b. Line blending

VUV survey spectrometers usually observe a wide range of energies, the SPRED instrument with the $450 g.mm^{-1}$ grating, for example, encompassing an order of magnitude range of photon energies. This is much larger than for visible spectrometers, whose energy range is at most a factor of 2. Such a wide energy range necessarily limits the spectral resolution that can be achieved by the VUV instruments, usually resulting in significant blending of the spectral lines. Line blending is perhaps the commonest cause of discrepancies in the VUV and so the possibility of line blending must be eliminated. This is particularly important for the CIV lines, which fall to shorter wavelengths where the problem is most severe. Of particular concern are blends with other C lines. In addition, lines from all impurities commonly found in JET, He, Be, N, O, Ne, Cl, Ar, Cr, Fe, Ni, and Cu have been considered. Both lists of spectral lines by Kelly (1987), supplemented by the current NIST listing (Ralchenko *et al*., 2007), and the higher resolution Schwob-Fraenkel spectra have been checked. Gas puffing of N, Ne or Ar can affect the temperature of the edge plasma and so pulses with gas puffing of impurity elements have already been excluded from the study. This means that only very intense lines that might still persist due to residual levels of these elements are of interest. The use of the limiter

phase of the discharge when C is both the dominant impurity and its lines are intense also minimizes problems due to blending.

For CIV there are only two blends of note, both affecting observations in the SPRED spectrum. The blending of a number of CIII lines with the 384.1Å line and of the NiXVIII transition at 292.0Å with the 289.2Å CIV line have been discussed in section 4a.

For CIII, one line at 585.5Å was rejected, because of a blend with HeI and this line would also be affected by residual Ar, there being a blend with ArVII. Blends between CIII and other C lines are discussed in section 4b.

Finally, it is noted that the CII line at 687.2Å is blended with the CIII line at 690.5Å. Although a comparison between modelled and measured results, as described in section 4c, suggests that the CIII component can be significant, it appears that the CII line normally dominates this blend.

c. Application of the collisional-radiative model and atomic data

In applying the collisional-radiative model to the CII to CIV ions, steady state conditions have been assumed. In the case of CIV, the time dependent rate equations, equations 1, have been solved to check the validity of this assumption. For electron densities typical of the SOL, $\leq 10^{19}\mathrm{m}^{-3}$, it was found that the populations of the excited levels were small, the $1s^2 2p$ levels having a population of $<2\times10^{-3} n_g$ and higher levels $\leq 10^{-6} n_g$, where n_g is the ground level population. The system is therefore close to the low density limit in which the dominant populating channel is collisional excitation from the ground level, followed by radiative decay. In this limit, the excited levels can be treated independently. This is reflected in the 1/e times required to reach steady state being close to the reciprocal of the transition probabilities of the depopulating radiative decays. Table 7 lists the 1/e values for the lowest 9 levels of CIV for densities of 10^{17} and $10^{19}\mathrm{m}^{-3}$, the lower density giving results identical to those found in the low density limit. They can be understood by reducing the set of interdependent rate equations, equations 1, to a single independent equation for n_i, by making the assumptions that $n_j q_{ji} << n_g q_{gi}$, $n_j A_{ji} << n_e n_g q_{gi}$ and $n_e q_{ij} << A_{ij}$. Hence,

$$\frac{dn_i}{dt} \approx n_e n_g q_{gi} - n_i \sum_{j<i} A_{ij}$$

and, solving for n_i,

$$n_i \approx \frac{n_e n_g q_{gi}}{\sum_{j<i} A_{ij}} \left(1 - \exp(-\sum_{j<i} A_{ij} t) \right),$$

the 1/e time being $1/\sum_{j<i} A_{ij}$. In table 7 it is noted that the 1/e values for the $3p^2P_{1/2}$ and $3p^2P_{3/2}$ levels are ~9% higher than expected from the transition probabilities. This is because the condition that $n_j A_{ji} << n_e n_g q_{gi}$ is not entirely satisfied, some additional population reaching the 3p levels via the radiative decay from the $4s^2S_{1/2}$ level. Setting the probabilities of transitions from the $4s^2S_{1/2}$ level to zero leads to agreement. Including even higher levels in the model leads to other similar discrepancies.

It is clear that the CIV ion reaches steady state conditions on time scales much faster than those associated with the plasma behaviour.

Further, it can be seen that in the low density limit, the steady state population is

$$n_i \approx \frac{n_e n_g q_{gi}}{\sum_{j<i} A_{ij}} ,$$

resulting in line intensity ratios of

$$\frac{I_{ij1}}{I_{kl1}} \approx \frac{q_{gi}A_{ij1}}{q_{gk}A_{kl1}} \frac{\sum_{l<k} A_{kl}}{\sum_{j<i} A_{ij}}.$$

For line ratios that involve lines in which a single transition dominates the radiative decay,

$$\frac{I_{ij}}{I_{kl}} \approx \frac{q_{gi}}{q_{gk}}.$$

It follows that the accuracy of the collisional excitation rates, in particular the rates of transitions from the ground level, can be more important than the accuracy of the transition probabilities, which in the low density limit can cancel. The transition probabilities are in any case independent of temperature and cannot explain a discrepancy that is temperature dependent.

Table 7. The 1/e times to reach steady state for the lowest 9 levels of CIV at T_e of 17.2eV

Level	Identification	$n_e = 10^{17}m^{-3}$ (s)	$n_e = 10^{19}m^{-3}$ (s)	$n_e = 10^{17}m^{-3}$, with A_{95} and $A_{96} = 0$ (s)	$1/\sum_{j<i} A_{ij}$ (s)
1	$1s^2 2s^2 S_{1/2}$	-	-	-	-
2	$1s^2 2p^2 P_{1/2}$	3.60e-9	3.59e-9	3.60e-9	3.62e-9
3	$1s^2 2p^2 P_{3/2}$	3.59e-9	3.57e-9	3.59e-9	3.60e-9
4	$1s^3 3s^2 S_{1/2}$	2.38e-10	2.38e-10	2.38e-10	2.37e-10
5	$1s^2 3p^2 P_{1/2}$	2.41e-10	2.44e-10	2.20e-10	2.20e-10
6	$1s^2 3p^2 P_{3/2}$	2.41e-10	2.44e-10	2.20e-10	2.20e-10
7	$1s^2 3d^2 D_{3/2}$	5.74e-11	5.84e-11	5.74e-11	5.73e-11
8	$1s^2 3d^2 D_{5/2}$	5.74e-11	5.84e-11	5.74e-11	5.73e-11
9	$1s^2 4s^2 S_{1/2}$	3.79e-10	3.79e-10	-	3.79e-10

The CIV atomic data used were generated specifically for this study and are regarded as being the best available over a wide temperature range (Aggarwal and Keenan, 2004). The transition probabilities are estimated to be accurate to better than 10% and the effective collision strengths, from which the rates are derived, to 20%. Figures 12 and 13 show that the 419.6Å, $2p^2P_{1/2,3/2} - 3s^2S_{1/2}$ transition has the strongest temperature dependence, increasing by 45% over the temperature range considered. The accuracies expected for the collisional rates do not explain this variation. Further, significant discrepancies in the description of the atomic physics, which might give rise to inaccuracies in the collisional rates, would also affect higher series members. The $2p^2P_{1/2,3/2} - 4s^2S_{1/2}$ transition is at 296.9Å and, although the data are more limited, they suggest a much smaller dependence in the opposite direction.

d. Ionization and recombination

In the collisional-radiative model presented in section 3, source terms, such as ionization and recombination, have been neglected. As was clear from the previous section, most of the population of the ion is in the ground level and the dominant ionization mechanism, electron collisional

ionization, proceeds from this level. Hence, this process will not affect the balance of the populations in the excited levels.

In contrast, the final state of the ion after recombination, whether dielectronic, radiative, three-body or charge-exchange, is likely to be an excited level, with the population of that level being increased. These processes have been included using the Photon Emissivity Coefficient (PEC), ε, formulation within the ADAS database. The contributions to the population and hence line intensities are divided into collisional excitation, recombination and charge exchange components (Summers, 2004),

$$I = n_e n_g \varepsilon^{exc} + n_e n_{g+1} \varepsilon^{rec} + n_D n_{g+1} \varepsilon^{cx},$$

where n_{g+1} is the ground level population of the next higher ionization stage and n_D the neutral D density, this ion giving rise to the most significant charge exchange contribution. The recombination PEC includes contributions representing dielectronic, radiative and three body recombination, although only the first two are expected to be significant at the densities of interest. No neutral beams were used during the limiter phase of the discharges and, hence, n_D is the density of the thermal neutral D background.

The charge exchange contribution to the 312.4Å (2s-3p) transition exceeds that to the 289.2Å (2p-4d) transition by several orders of magnitude. Consequently, it is difficult to see how charge exchange could be a satisfactory explanation of the discrepancies given the similarity of the dependencies of the 419.6Å/312.4Å (2p-3s)/(2s-3p) and 419.6Å/289.2Å (2p-3s)/(2p-4d) ratios, shown in figures 12 and 13, respectively. The recombination PECs for the 312.4Å and 289.2Å transitions are much closer, but still differ by a factor of 2, the non-charge exchange recombinations being more important for the 289.2Å (2p-4d) transition.

Nevertheless, detailed checks were made to see if the inclusion of recombination enabled the observed measurements of the CIV 312.4Å/289.2Å (2s-3p)/(2p-4d), 419.6Å/312.4Å (2p-3s)/(2s-3p) and 384.1Å/312.4Å (2p-3d)/(2s-3p) line intensity ratios to be satisfactorily described. Charge exchange recombination and dielectronic and radiative recombination, the latter two grouped together in the recombination PEC, were considered both separately and together.

In the case of charge exchange recombination, the equation

$$\frac{I_1}{I_2} = \frac{\varepsilon_1^{exc} + n_{cx}.\varepsilon_1^{cx}}{\varepsilon_2^{exc} + n_{cx}.\varepsilon_2^{cx}},$$

where n_{cx} corresponds to the temperature dependent ratio of densities $\frac{n_D n_{g+1}}{n_e n_g}$, was solved for the 312.4Å/289.2Å and 384.1Å/312.4Å ratios to obtain n_{cx} and the appropriate electron temperature; the latter will be different from that derived without recombination. This was done for particular values of the sensitivity calibration at 384.1Å and for a range of measured input ratios, the fits to the discrepancies as given by equation 2, being used to derive these ratios so as to minimize measurement errors. The sensitivity calibration at 419.6Å was then determined from the 419.6Å/312.4Å ratio. Figure 17 shows the results of two calculations with the 384.1Å inverse sensitivity fixed at 1.4 and 1.8 relative to that at 312.4Å. The first sensitivity used is close to that from the independent analysis of the Na- and Li-like doublets, the latter close to the mean value derived from the CIV analysis. In the figure the derived inverse sensitivity calibrations at 419.6Å are plotted against the temperature found from the 312.4Å/289.2Å ratio before the inclusion of charge exchange. These calculations were made

for an electron density of $10^{18}m^{-3}$, although between densities of 10^{17} to $10^{19}m^{-3}$ no significant dependence on density was found. It can be seen that the derived sensitivity at 419.6Å is still dependent on electron temperature and no parameter space was found were this was not the case. The values of n_{cx}, together with the temperatures and the derived 'inverse sensitivity' are given in table 8. The lower the 384.1Å inverse sensitivity chosen the higher the electron temperature needed to give consistent results. For a sensitivity close to that found from the independent calibration, the temperature reaches 48eV and up to 35% of the population in the $1s^2 3p\ ^2P$ levels, the upper levels of the 312.4Å transition, is due to charge exchange recombination; neither would be expected. It is noted that a 10% error was allowed in the fits used to see if the temperature dependence of the 419.6Å sensitivity could be reduced, but with no significant effect.

Table 8. Results after the inclusion of charge exchange (CX) recombination into the model.

T_e derived without CX	S^{-1} at 384.1Å of 1.4			S^{-1} at 384.1Å of 1.8		
	T_e derived with CX	n_{cx}	S^{-1} at 419.6Å	T_e derived with CX	n_{cx}	S^{-1} at 419.6Å
11.0	19.0	0.0360	2.16	11.5	0.0021	3.66
11.5	20.0	0.0350	2.07	12.0	0.0025	3.45
12.0	22.0	0.0352	1.94	13.0	0.0044	3.15
12.5	24.0	0.0350	1.82	14.0	0.0060	2.91
13.0	26.0	0.0344	1.72	15.0	0.0073	2.72
13.5	28.0	0.0334	1.63	16.0	0.0084	2.55
14.0	31.0	0.0319	1.54	17.0	0.0094	2.40
14.5	38.0	0.0278	1.42	18.0	0.0102	2.27
15.0	48.0	0.0218	1.30	19.5	0.0116	2.12

A similar procedure was used for dielectronic and radiative recombination, except that the 312.4Å/289.2Å and 384.1Å/312.4Å ratios were used to give the ratio of the ground level densities, n_{g+1}/n_g, and T_e. In this case, there is some density dependence and hence the calculations were carried out at densities of 10^{17}, 10^{18} and $10^{19}m^{-3}$, but no satisfactory solutions were found; either the temperature found was particularly low, often ≤ 5eV, the ground level density ratio very high, > 20, or negative for some or all of the input data.

Finally the effect of adding dielectronic and radiative recombination to a case with charge exchange was tested to see if this allowed the observed temperature dependence of the 419.6Å sensitivity to be reduced. For ratios of the ground level densities up to ~20, the changes were small, but if anything marginally increased the temperature dependence.

It is concluded that although the various recombinations, particularly charge exchange recombination, will have some contribution to the level populations, their inclusion does not allow the discrepancies presently being discussed to be explained. Including charge exchange recombination will tend to increase the temperature derived for the emitting region of the CIV ion.

e. Non-Maxwellian electron energy distribution

In attempting to explain the discrepancies between the measured and modelled line intensity ratios, consideration is also being given to the possibility of a non-Maxwellian electron energy

distribution in the SOL. Although a fluid analysis, in which the particle energy distributions are taken to be Maxwellian, is normally found to be appropriate, the fluid approximation can be marginal, this depending on the temperature and density of the region of the plasma emitting the CIV radiation.

The electron collisional rate for a transition from state i to j, q_{ij}, used in the collisional-radiative model is usually derived from the collision strength, $\Omega_{ij}(E_j)$, calculated as a function of the electron impact energy relative to the final state j of the transition E_j, assuming that the electron energy distribution is Maxwellian,

$$q_{ij} = 8.63x10^{-12} \frac{\gamma_{ij} \exp(-E_{ij} / kT_e)}{\omega_i T_e^{1/2}} \text{ m}^3.\text{s}^{-1},$$

where the effective collision strength

$$\gamma_{ij} = \int_0^\infty \Omega_{ij} \exp\left(-\frac{E_j}{kT_e}\right) d\left(\frac{E_j}{kT_e}\right),$$

E_{ij} is the transition energy and ω_i the statistical weight of the initial state.

Collisional rates have been calculated using non-Maxwellian electron energy distributions, which allow some of the discrepancies to be reduced. At this stage it is not clear whether the agreement is fortuitous and this work is continuing.

f. Dependence on plasma parameters

A search was made for a correlation between the discrepancy observed for CIV and various plasma parameters. The toroidal field, plasma current, q_{95} and LIDAR measurements of electron density and temperature near to the edge of the plasma were checked, but no correlation found. It should be noted, however, that the steep edge gradients mean that the density and temperature routinely available on JET from LIDAR measurements may only correlate weakly with the actual density and temperature of the CIV emitting plasma region. Neither was any correlation found with plasma position. Most, although not all of the plasmas, were limited on the outer poloidal limiters.

6. Conclusions

Comparisons between measured and modelled CII to CIV VUV spectral line intensity ratios have a more limited accuracy than expected, with discrepancies of up to ~45% being found. The discrepancies occur between series of pulses and, in some cases, even during a pulse, with the 419.6Å CIV line in particular being found to be exceptional. This is contrasted with the comparisons of the Li- and Na-like doublets of various elements made by Lawson *et al*. (2008), for which the agreement was limited only by the experimental errors. A better understanding of the limitation in the modelling of the C ratios has been sought. Line blending, the steady state approximation normally used in the collisional-radiative model and recombination affecting the level populations have been considered, the CIV ionization stage being most thoroughly investigated. However, as yet no satisfactory explanation of the discrepancies has been found. Use of non-Maxwellian electron energy distributions in determining the electron collisional rates have allowed the discrepancies to be reduced, although at present it is not possible to say whether this is just fortuitous. Further work is to be carried out to complete the study. Consideration is also being given to the effect of the line of sight integration

through a plasma region with steep gradients and whether this might explain the discrepancies (Zacks, 2008).

In the present analysis, only ohmic, limiter pulses viewed along a horizontal line of sight have been considered, but similar discrepancies are seen both during the limiter and additionally heated, X-point phases of the discharge with another VUV spectrometer on JET, which has a vertical line of sight (Zacks, 2008). An analysis of C data from a lower temperature machine than JET, in which the CIV ionization stage is emitted from the core rather than the edge plasma could be advantageous in showing whether the discrepancies are linked to the plasma region.

The authors would like to express their particular thanks for helpful discussions with Drs. I. Ksiazek, L. Lauro-Taroni and L. Ryc.

This work was carried out within the framework of the European Fusion Development Agreement and was partly funded by the United Kingdom Engineering and Physical Sciences Research Council and by the European Communities under the contract of Association between EURATOM and UKAEA. The views and opinions expressed herein do not necessarily reflect those of the European Commission.

* See the Appendix of M L Watkins et al., Fusion Energy, 2006, (Proc. 21st Int. Conf. Chengdu, 2006) IAEA, (2006)

References

Aggarwal K M and Keenan F P, 2004, Phys. Scr., **69**, 385

Allard N, Artru M-C, Lanz T and Le Dourneuf M, 1990, Astron. Astrophys. Suppl. Ser., **84**, 563

Berrington K A, 1994, ADNDT, **57**, 71

Coffey I H, Barnsley R *et al.*, 2004, Rev. Sci. Instrum., **75**, 3737

Coffey I H *et al*., 2009, to be submitted to J. Instrum.

Fonck R J, Ramsey A T, Yelle R V, 1982, Appl. Opt., **21**, 2115

Griffin D C, Badnell N R, Pindzola M S, 2000, J. Phys. B, **33**, 1013

Kelly R L, 1987, J. Phys. Chem. Ref. Data, **16**, Suppl. 1

Lawson K D and Peacock N J, 1988, Opt. Commun. **68**, 121

Lawson K D, Peacock N J, Hawkes N C, Behringer K, Denne G B, Patel T K, Prince S, Siewecke F, 1987, 'Validation of KT2 data and the SAS, spectroscopic database', TAN(87)1-3

Lawson K D *et al*., 2008, to be submitted to J. Instrum.

Nussbaumer H and Storey P J, 1978, Astron. Astrophys., **64**, 139

Ralchenko Yu, Jou F-C, Kelleher D E, Kramida A E, Musgrove A, Reader J, Wiese W L and Olsen K, 2007, NIST Atomic Spectra Database (version 3.1.2), http://physics.nist.gov/asd3

Sampson D H, Zhang H L and Fontes C J, 1994, ADNDT, **57**, 97

Schwob J L, Wouters A W, Suckewer S, Finkenthal M, 1987, Rev. Sci. Instrum., **58**, 1601

Summers H P, 2004, 'The ADAS User Manual, version 2.6, http://adas.phys.strath.ac.uk'

Zacks J, 2008, Ph. D. Thesis.

Figure captions

Figure 1. The SPRED spectrum for JET pulse 63445 averaged between times 4 and 10s.
Figure 2. The Schwob-Fraenkel spectrum recorded with the 300g.mm^{-1} grating for JET pulse 52597 averaged between times 4 and 10s.
Figure 3. The Schwob-Fraenkel spectrum recorded with the 600g.mm^{-1} grating for JET pulse 58259 averaged between times 5 and 12s.
Figure 4. Ratio of the derived 'inverse sensitivity' at 419.6Å to that at 312.4Å plotted against the electron temperature as measured by the 312.4Å/289.2Å line intensity ratio.
Figure 5. Time histories of the 289.2Å, 312.4Å and 419.6Å line intensities in JET pulse 56907.
Figure 6a. T_e derived from the 289.2Å/244.9Å line ratio plotted against T_e from the 312.4Å/289.2Å ratio. The line is derived from fits to the discrepancies.
Figure 6b. Ratio of T_e derived from the 289.2Å/244.9Å and 312.4Å/289.2Å line ratios plotted against T_e from the 312.4Å/289.2Å ratio. The line is derived from fits to the discrepancies.
Figure 7a. T_e derived from the 312.4Å/296.9Å line ratio plotted against T_e from the 312.4Å/289.2Å ratio. The line is derived from fits to the discrepancies.
Figure 7b. Ratio of T_e derived from the 312.4Å/296.9Å and 312.4Å/289.2Å line ratios plotted against T_e from the 312.4Å/289.2Å ratio. The line is derived from fits to the discrepancies.
Figure 8a. T_e derived from the 384.1Å/419.6Å line ratio plotted against T_e from the 384.1Å/289.2Å ratio. The line is derived from fits to the discrepancies.
Figure 8b. Ratio of T_e derived from the 384.1Å/419.6Å and 384.1Å/289.2Å line ratios plotted against T_e from the 384.1Å/289.2Å ratio. The line is derived from fits to the discrepancies.
Figure 9a. T_e derived from the 384.1Å/289.2Å line ratio plotted against T_e from the 312.4Å/289.2Å ratio. The line is derived from fits to the discrepancies.
Figure 9b. Ratio of T_e derived from the 384.1Å/289.2Å and 312.4Å/289.2Å line ratios plotted against T_e from the 312.4Å/289.2Å ratio. The line is derived from fits to the discrepancies.
Figure 10a. T_e derived from the 312.4Å/296.9Å line ratio plotted against T_e from the 384.1Å/289.2Å ratio. The line is derived from fits to the discrepancies.
Figure 10b. Ratio of T_e derived from the 312.4Å/296.9Å and 384.1Å/289.2Å line ratios plotted against T_e from the 384.1Å/289.2Å ratio. The line is derived from fits to the discrepancies.
Figure 11a. T_e derived from the 384.1Å/244.9Å line ratio plotted against T_e from the 384.1Å/289.2Å ratio. The line is derived from fits to the discrepancies.
Figure 11b. Ratio of T_e derived from the 384.1Å/244.9Å and 384.1Å/289.2Å line ratios plotted against T_e from the 384.1Å/289.2Å ratio. The line is derived from fits to the discrepancies.
Figure 12. Discrepancy (d) for the 419.6Å/312.4Å line ratio plotted against T_e from the 312.4Å/289.2Å ratio. The line is a straight line fit made to the points +.
Figure 13. Discrepancy (d) for the 419.6Å/289.2Å line ratio plotted against T_e from the 312.4Å/289.2Å ratio. The line is a straight line fit made to the points +.
Figure 14. Discrepancy (d) for the 384.1Å/312.4Å line ratio plotted against T_e from the 312.4Å/289.2Å ratio. The line is a straight line fit made to the points +.
Figure 15. Discrepancy (d) for the 296.9Å/312.4Å line ratio plotted against T_e from the 312.4Å/289.2Å ratio. The line is a straight line fit made to the points +.
Figure 16. Discrepancy (d) for the 244.9Å/312.4Å line ratio plotted against T_e from the 312.4Å/289.2Å ratio. The line is a straight line fit made to the points +.

Figure 17. Ratio of the derived 'inverse sensitivity' at 419.6Å to that at 312.4Å plotted against the electron temperature as measured by the 312.4Å/289.2Å line intensity ratio. + calculation uses S^{-1} at 384.1Å of 1.4 and + S^{-1} at 384.1Å of 1.8.

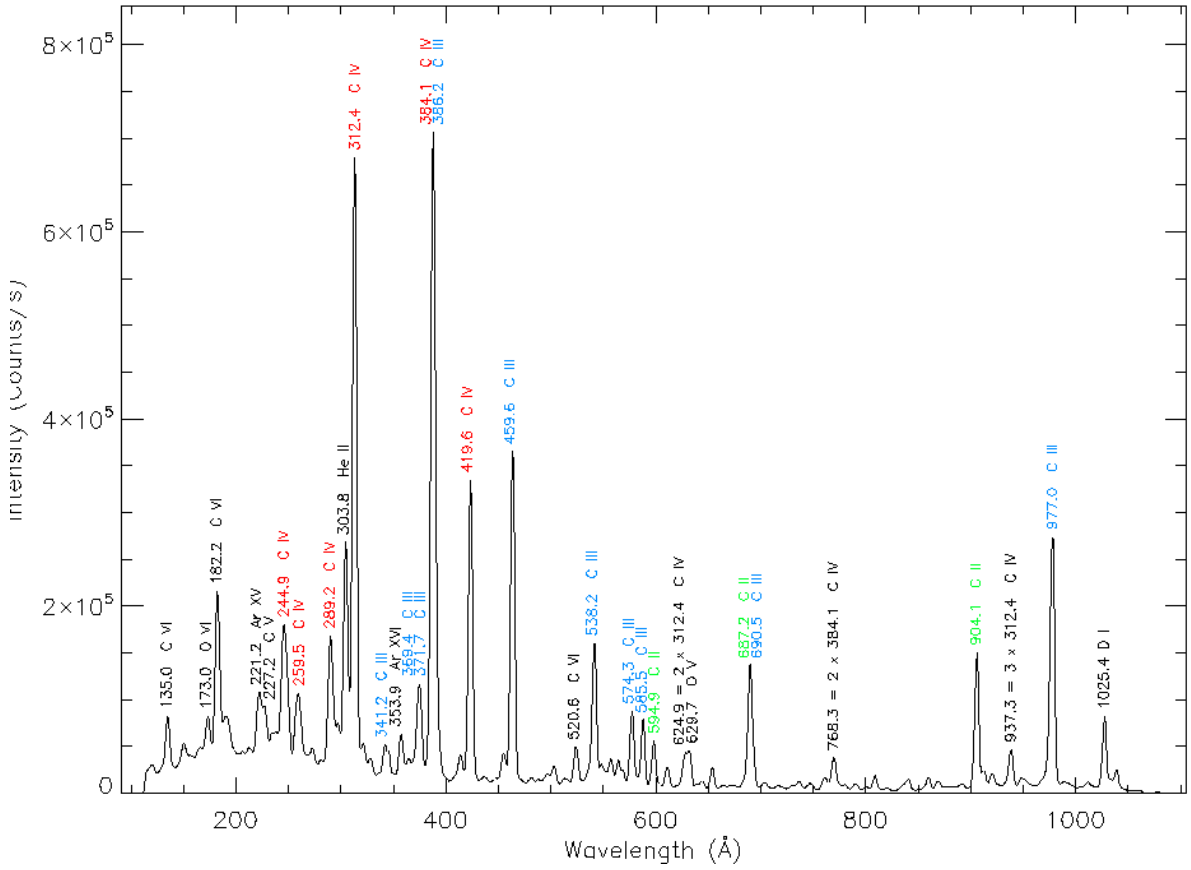

Figure 1.

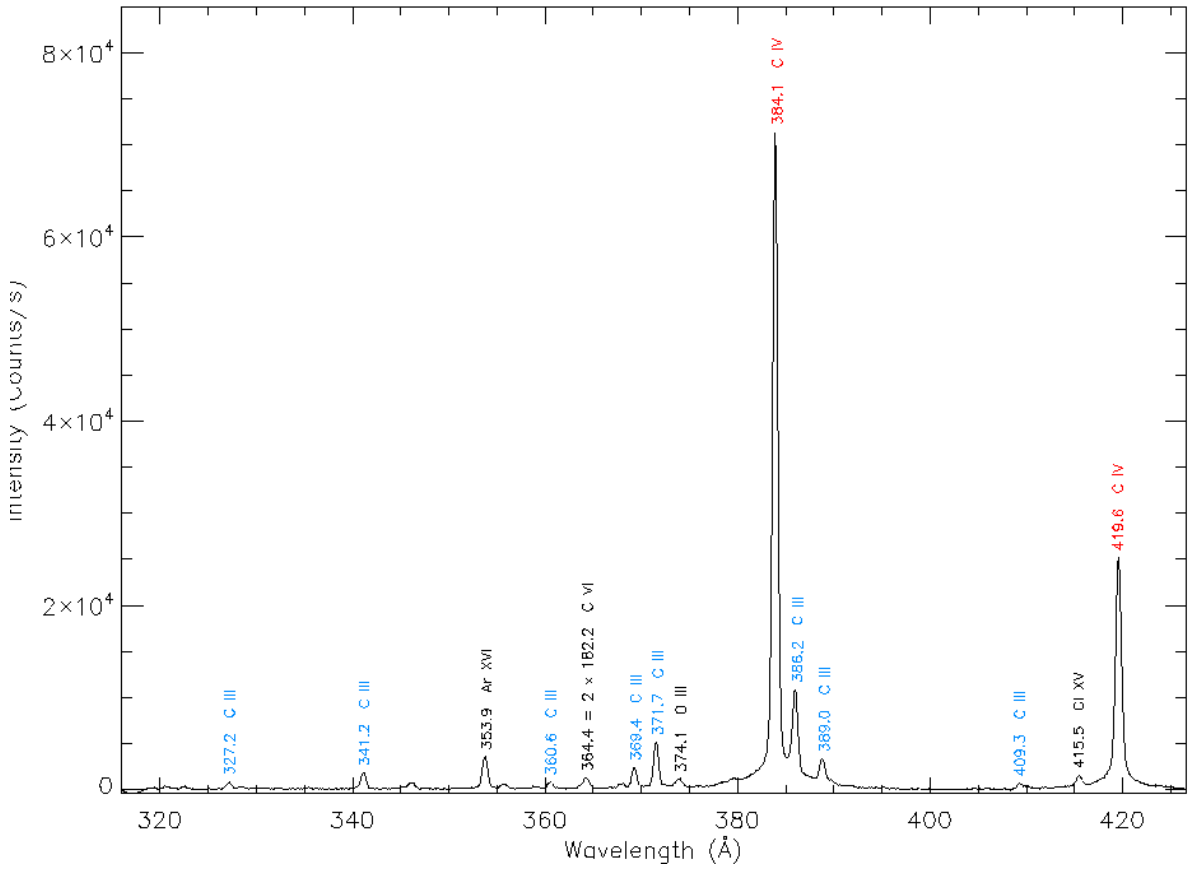

Figure 2.

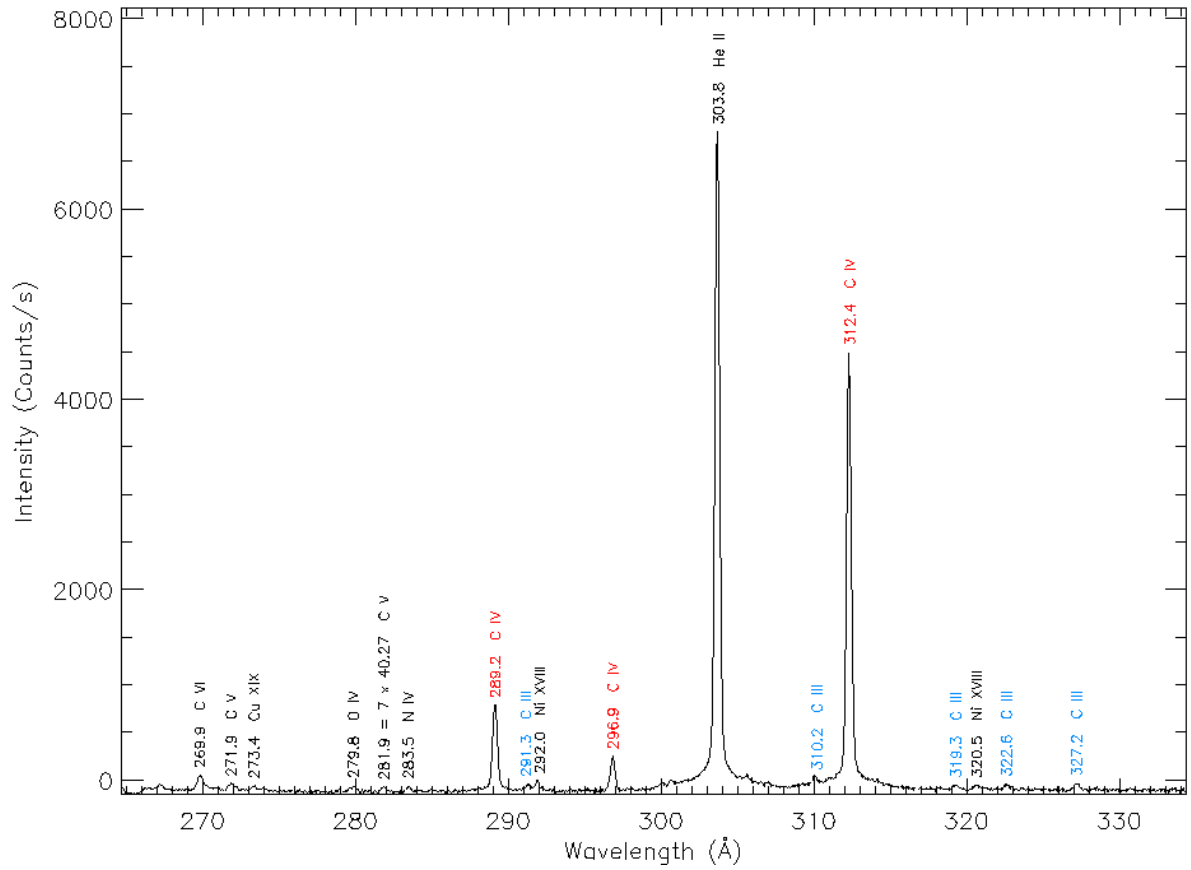

Figure 3.

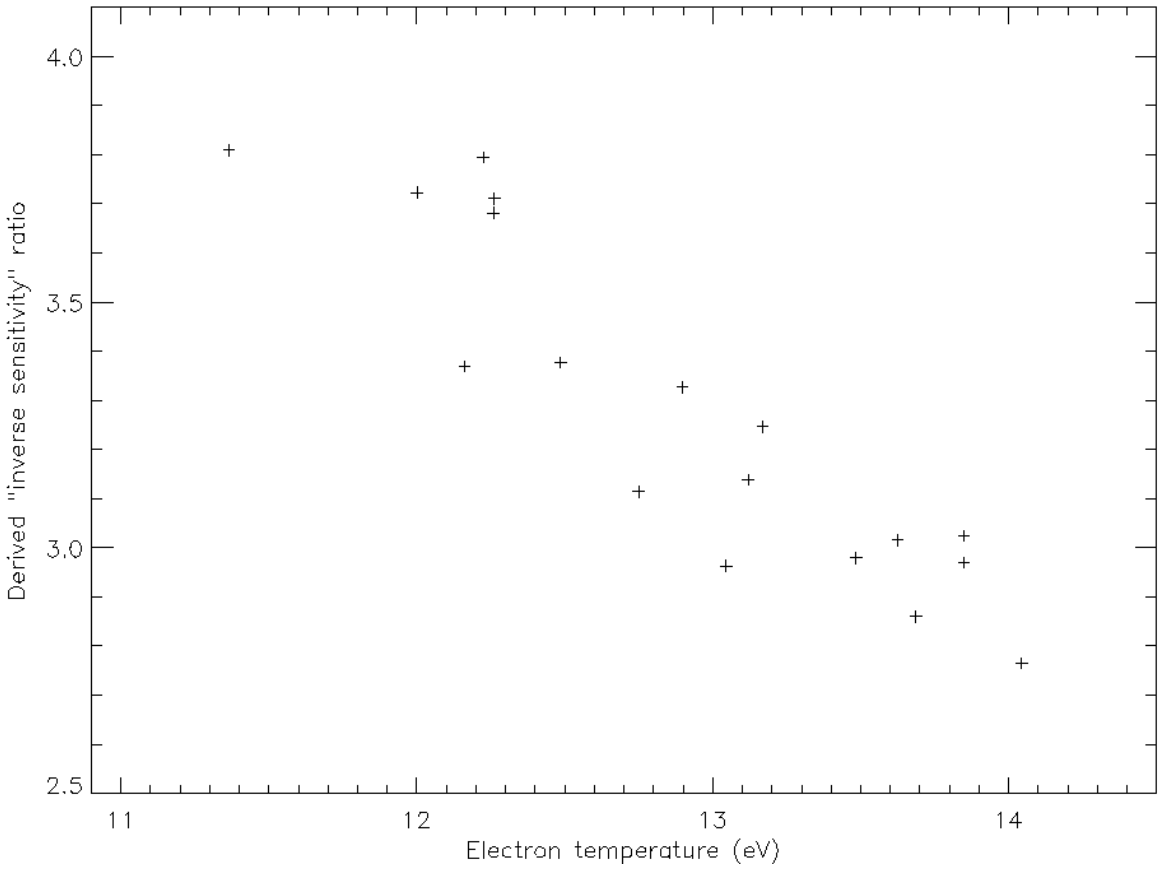

Figure 4.

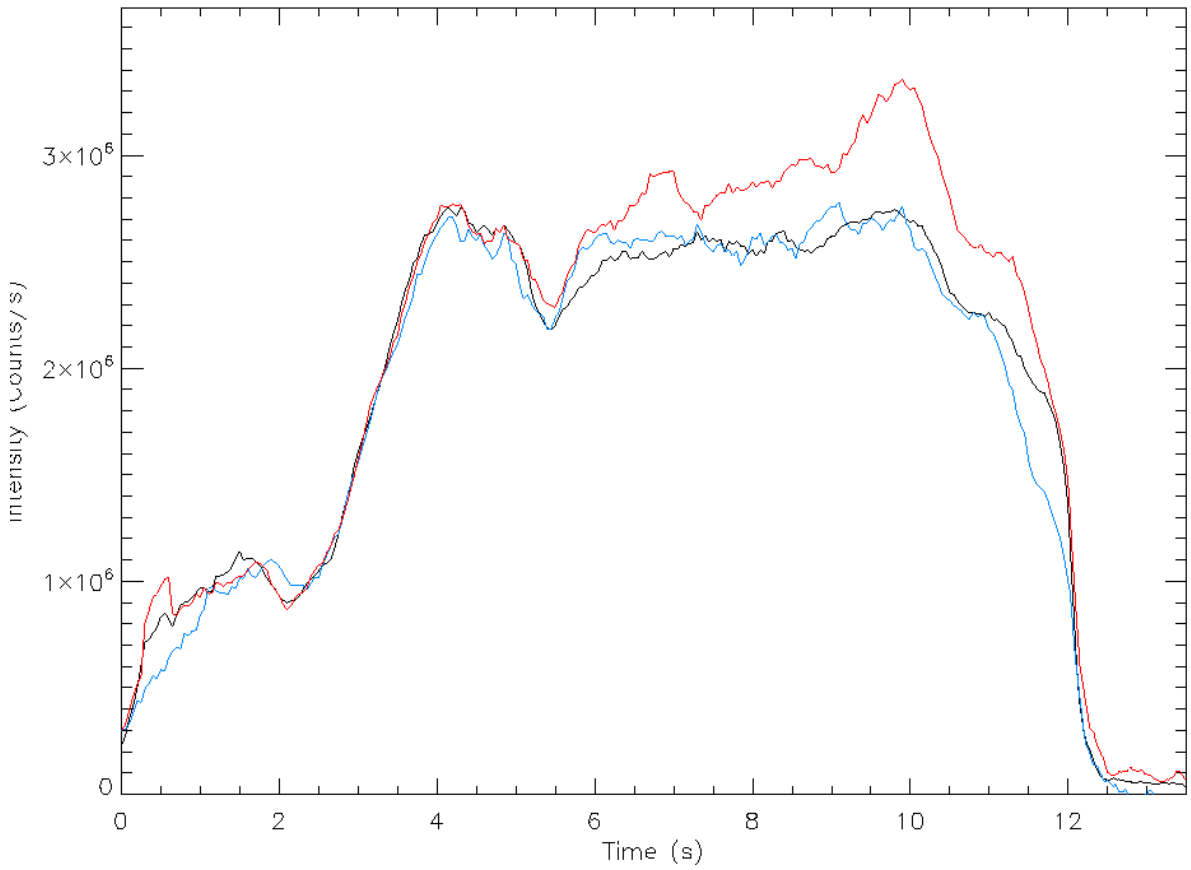

Figure 5.

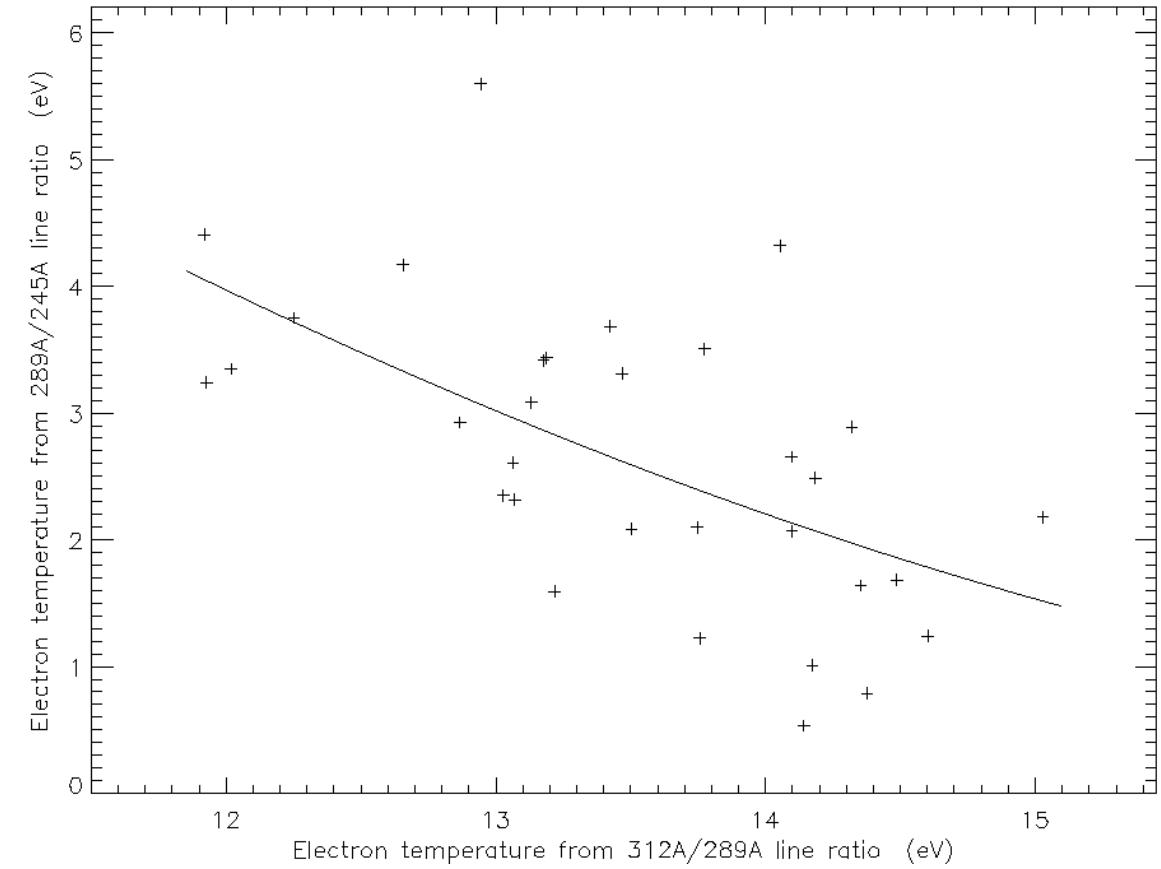

Figure 6a.

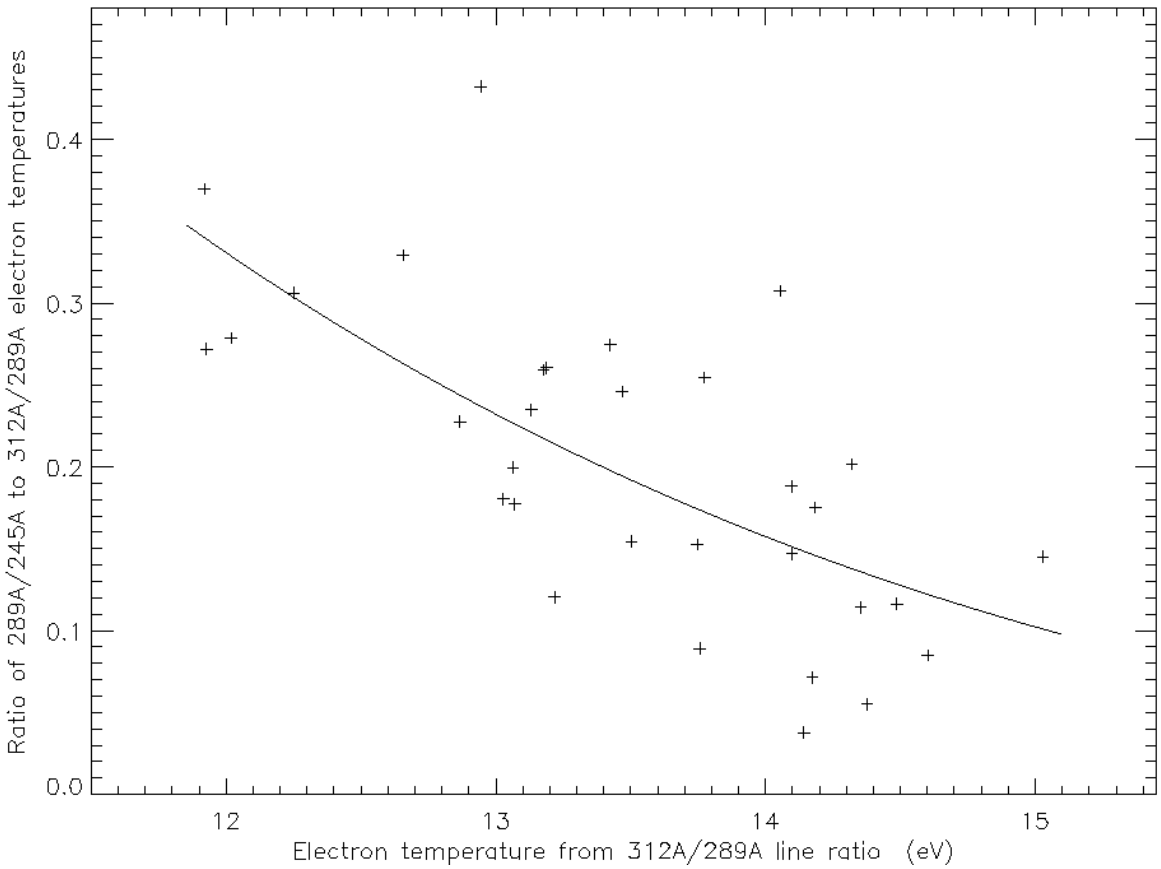

Figure 6b.

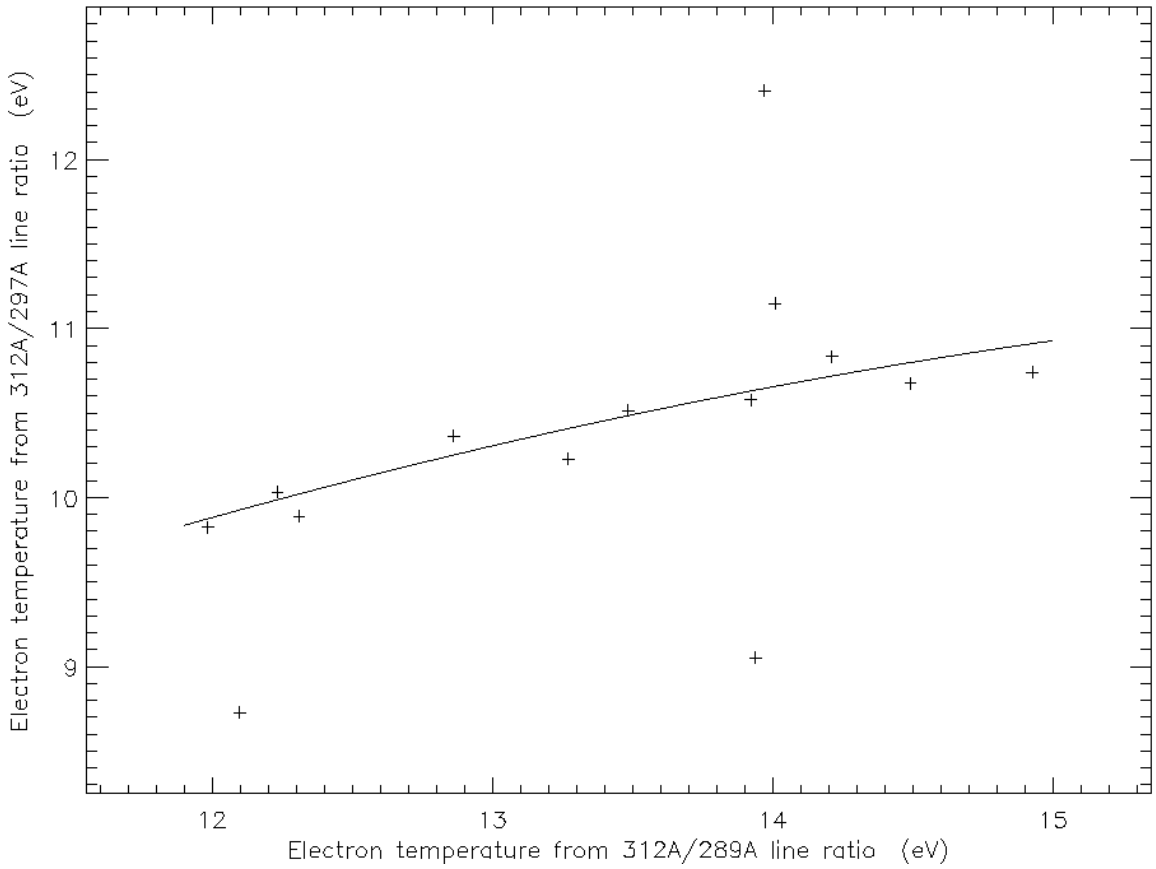

Figure 7a.

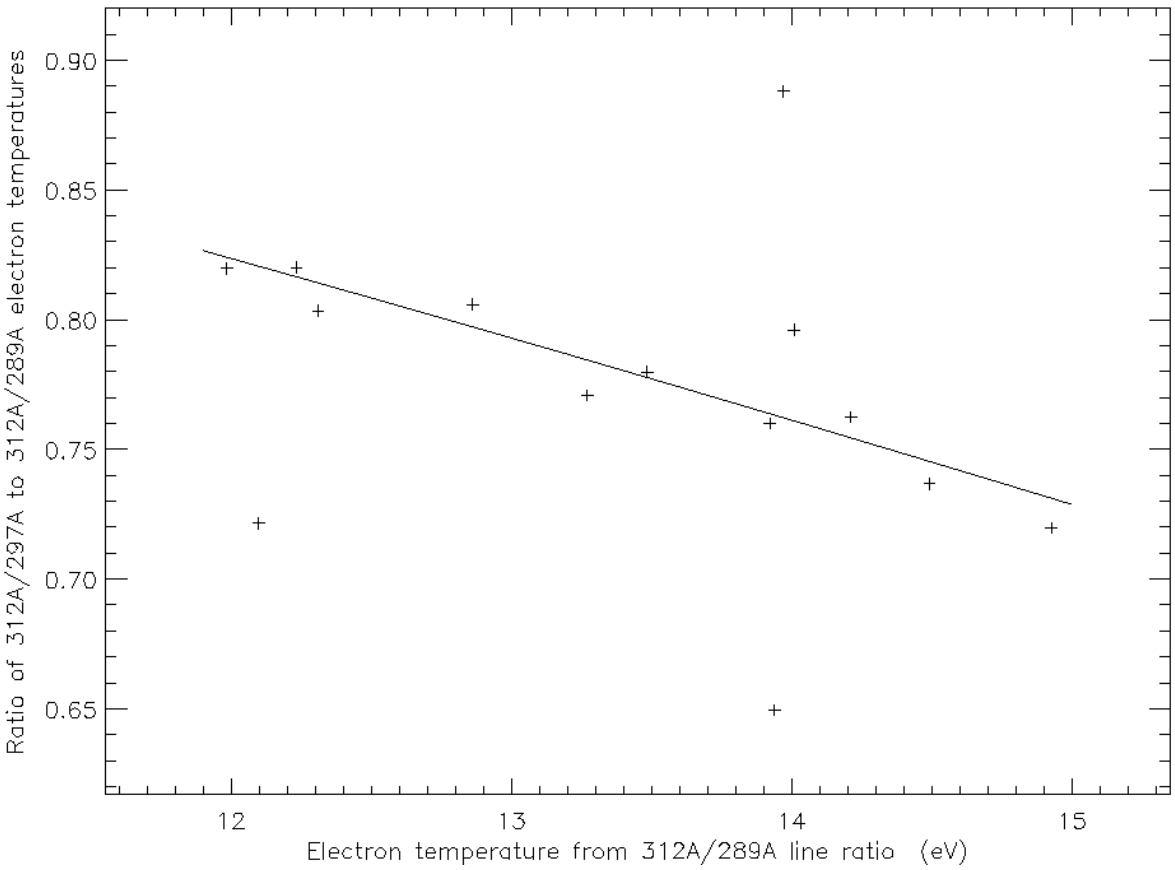

Figure 7b.

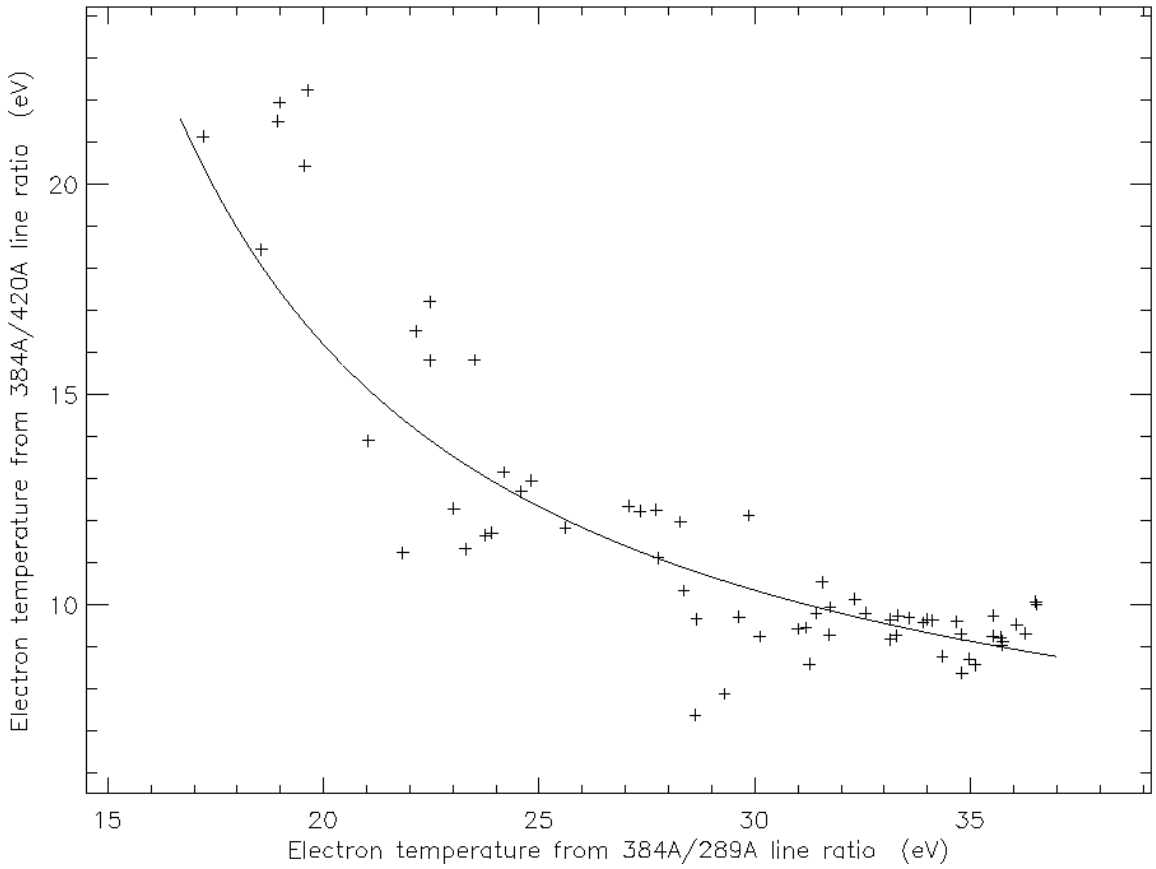

Figure 8a.

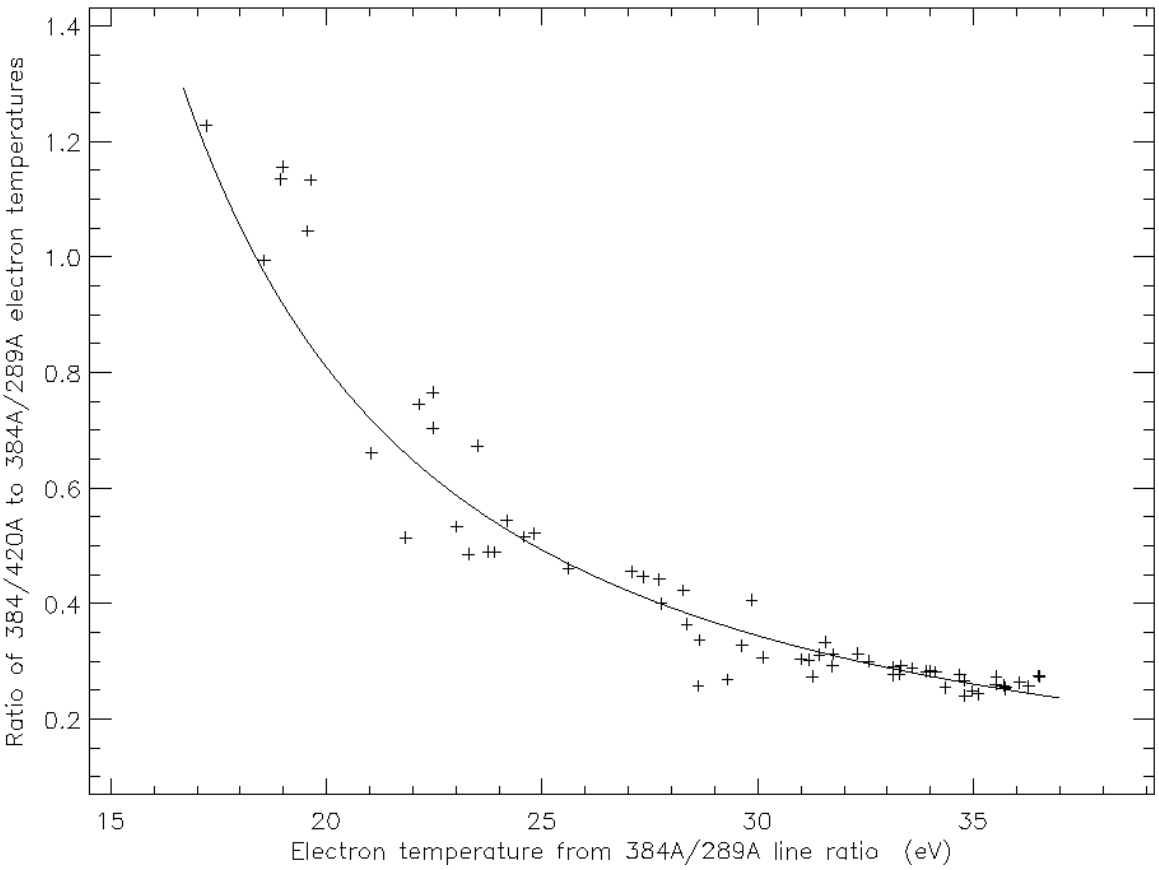

Figure 8b.

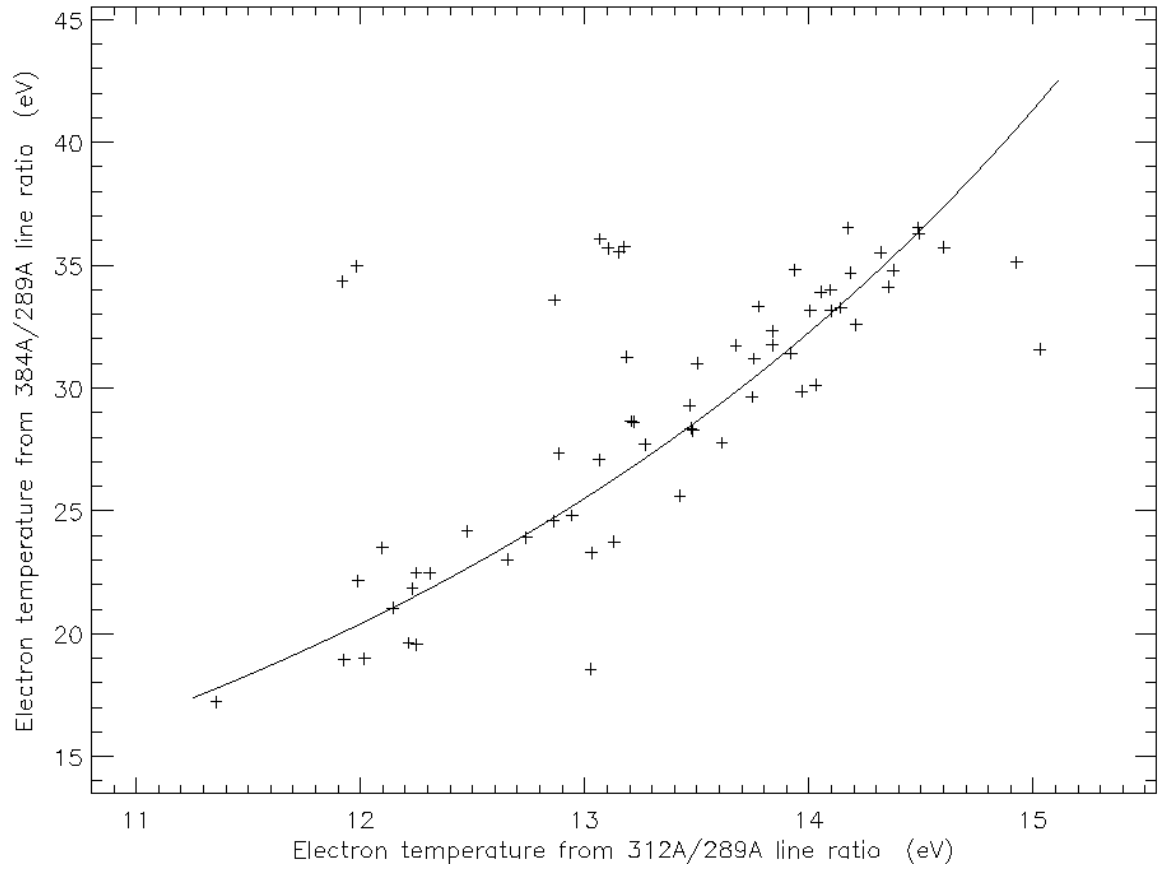

Figure 9a.

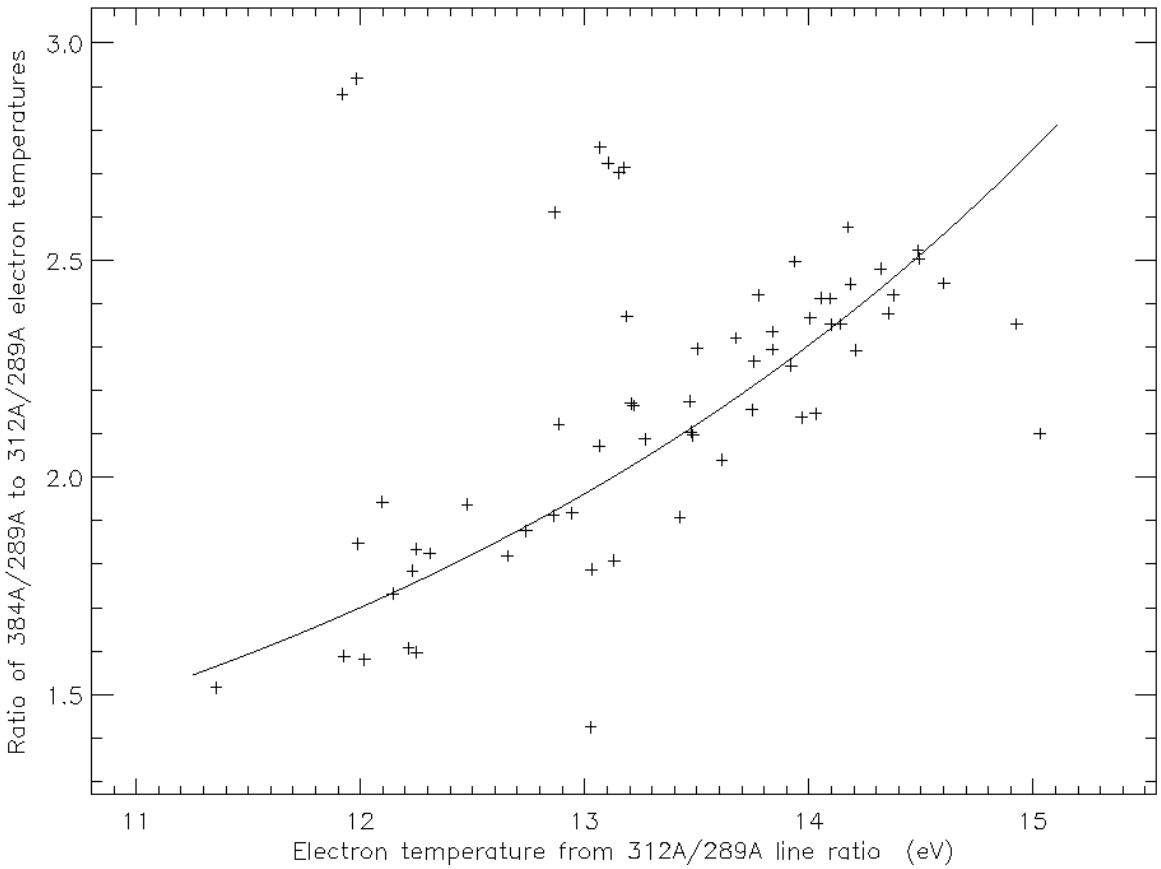

Figure 9b.

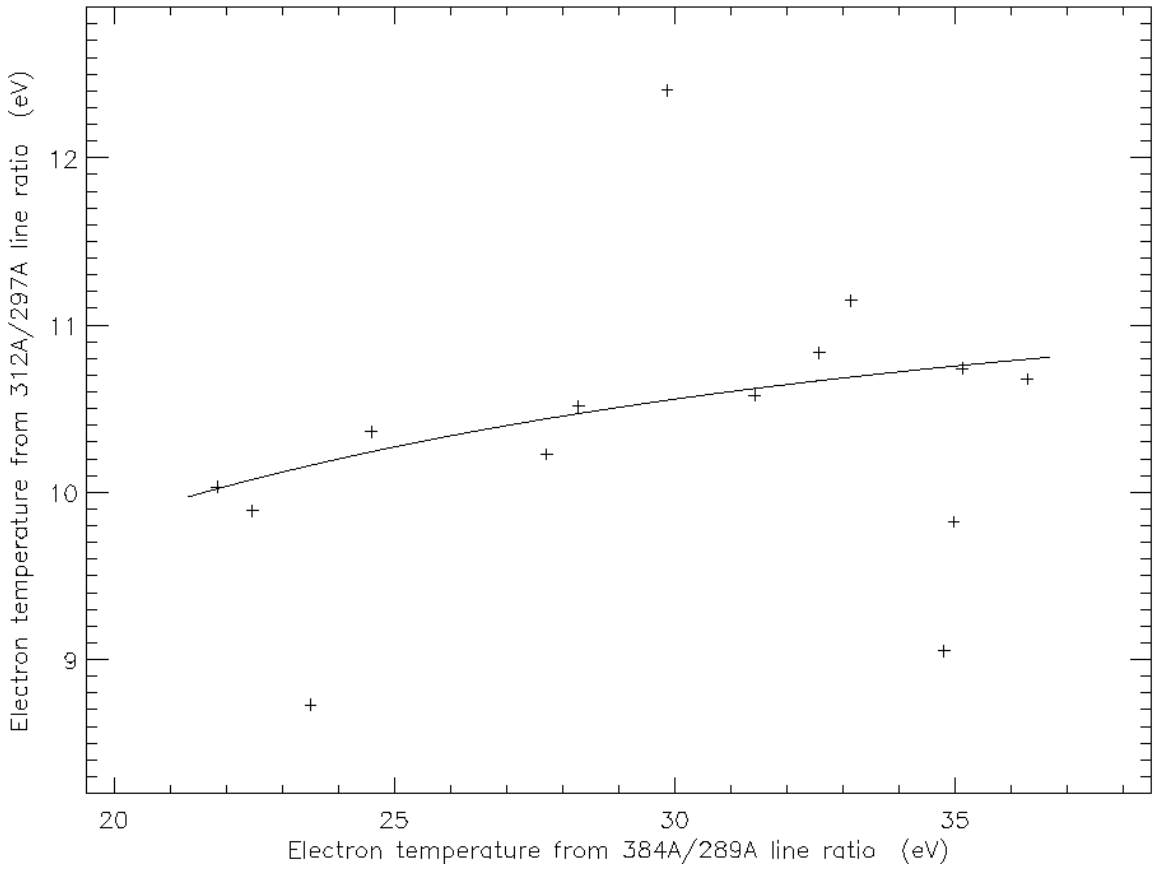

Figure 10a.

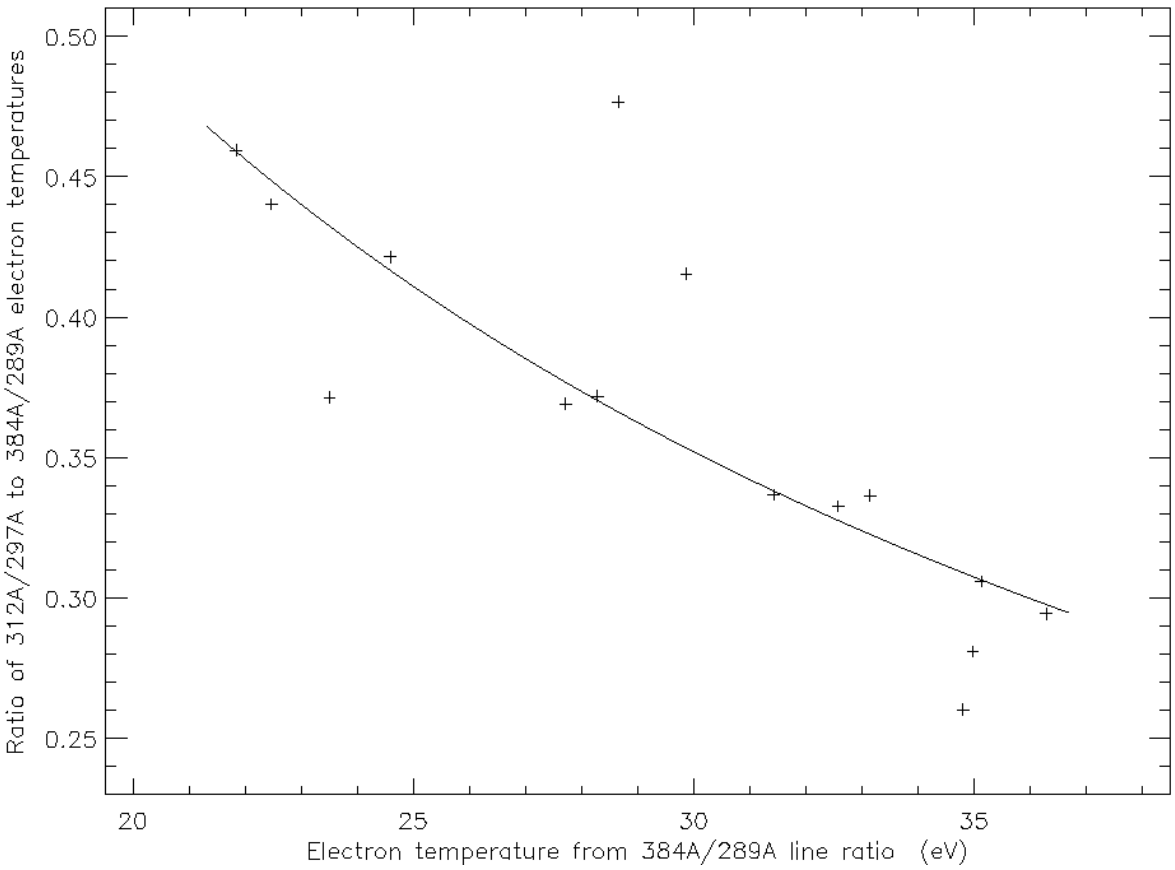

Figure 10b.

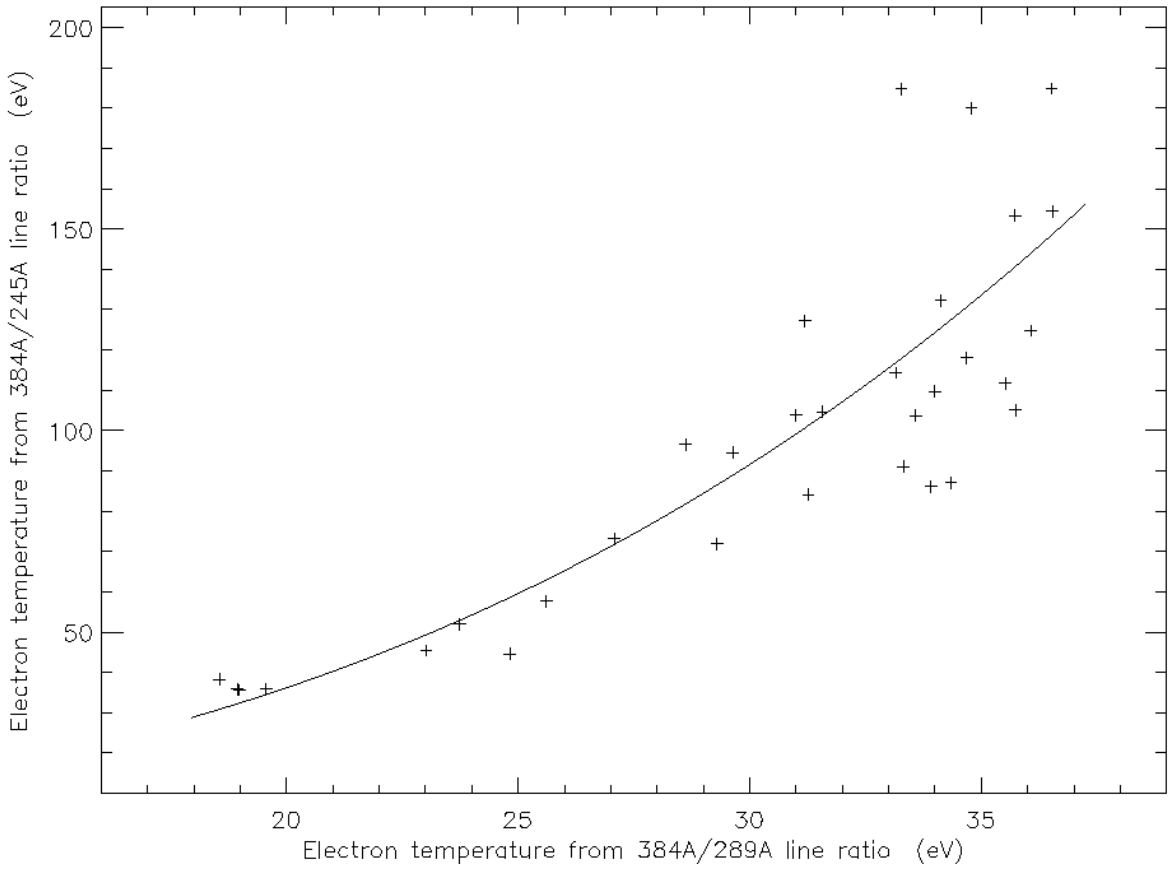

Figure 11a.

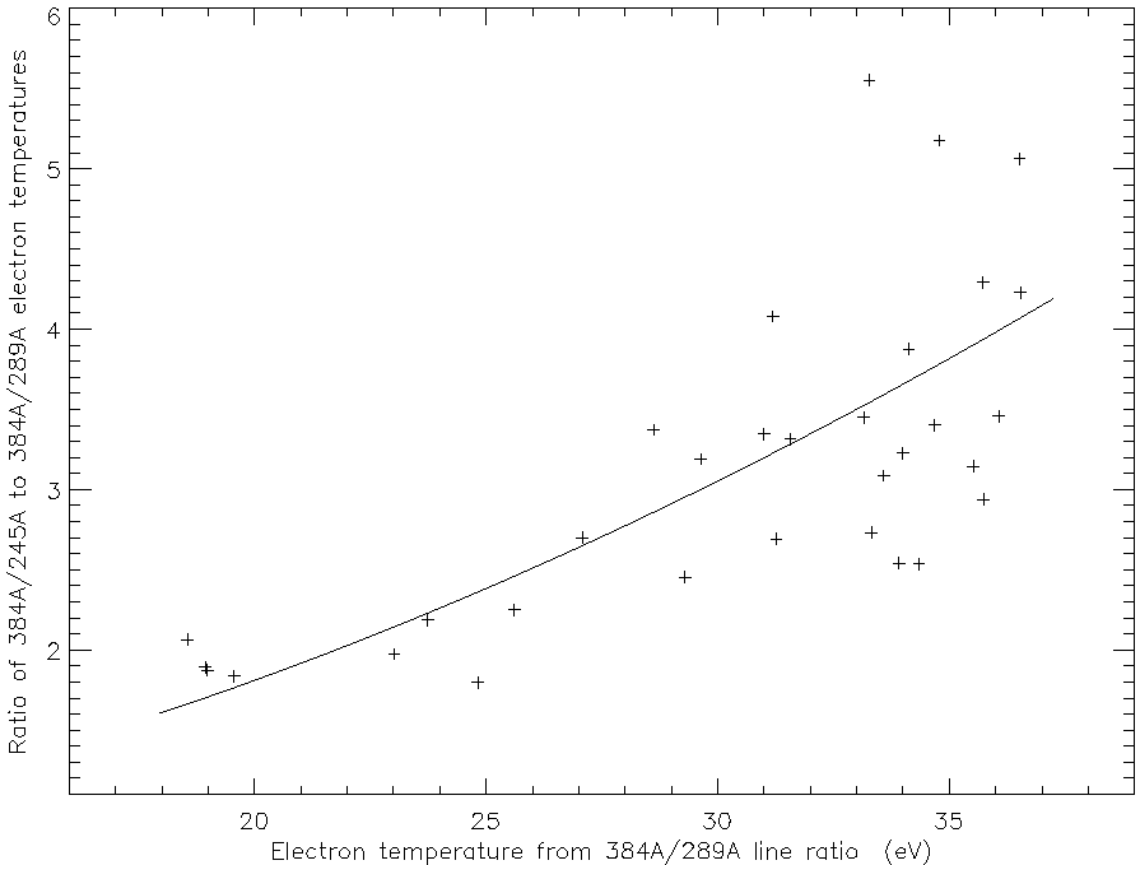

Figure 11b.

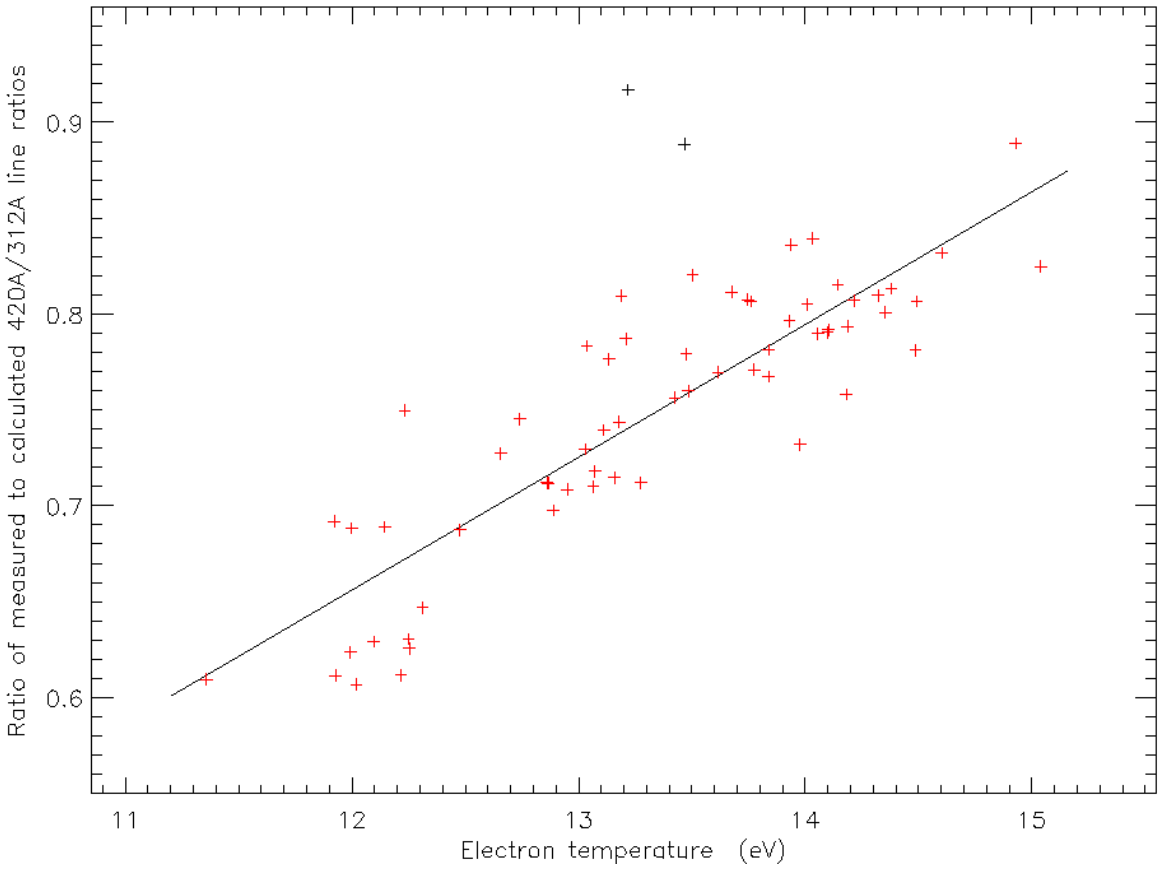

Figure 12.

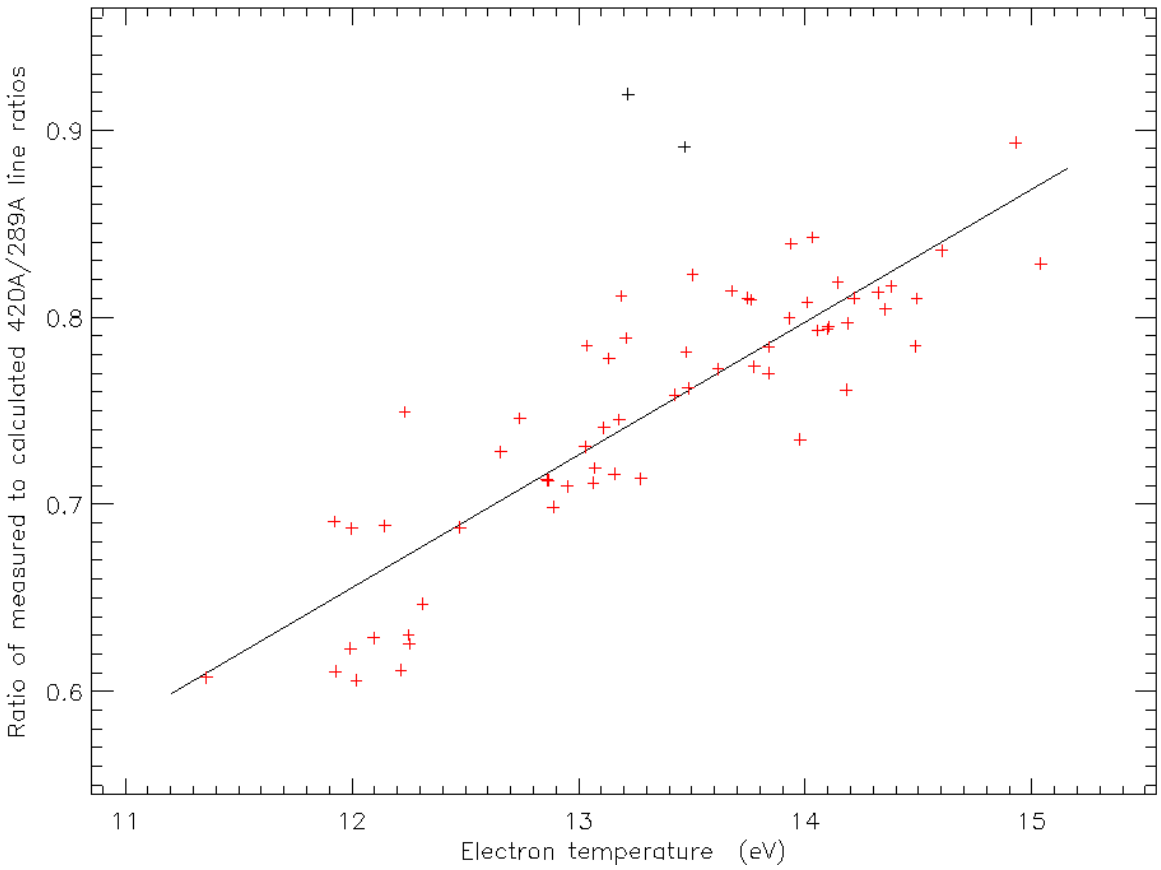

Figure 13.

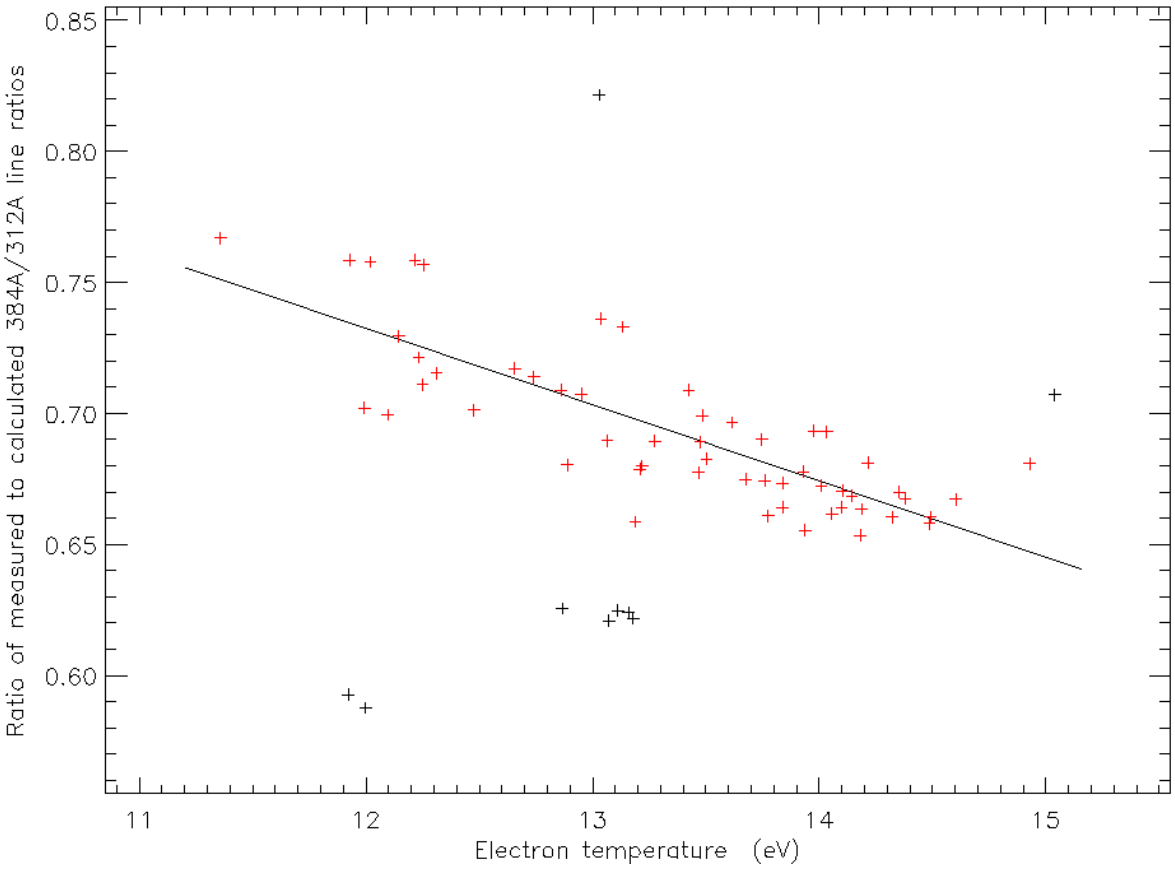

Figure 14.

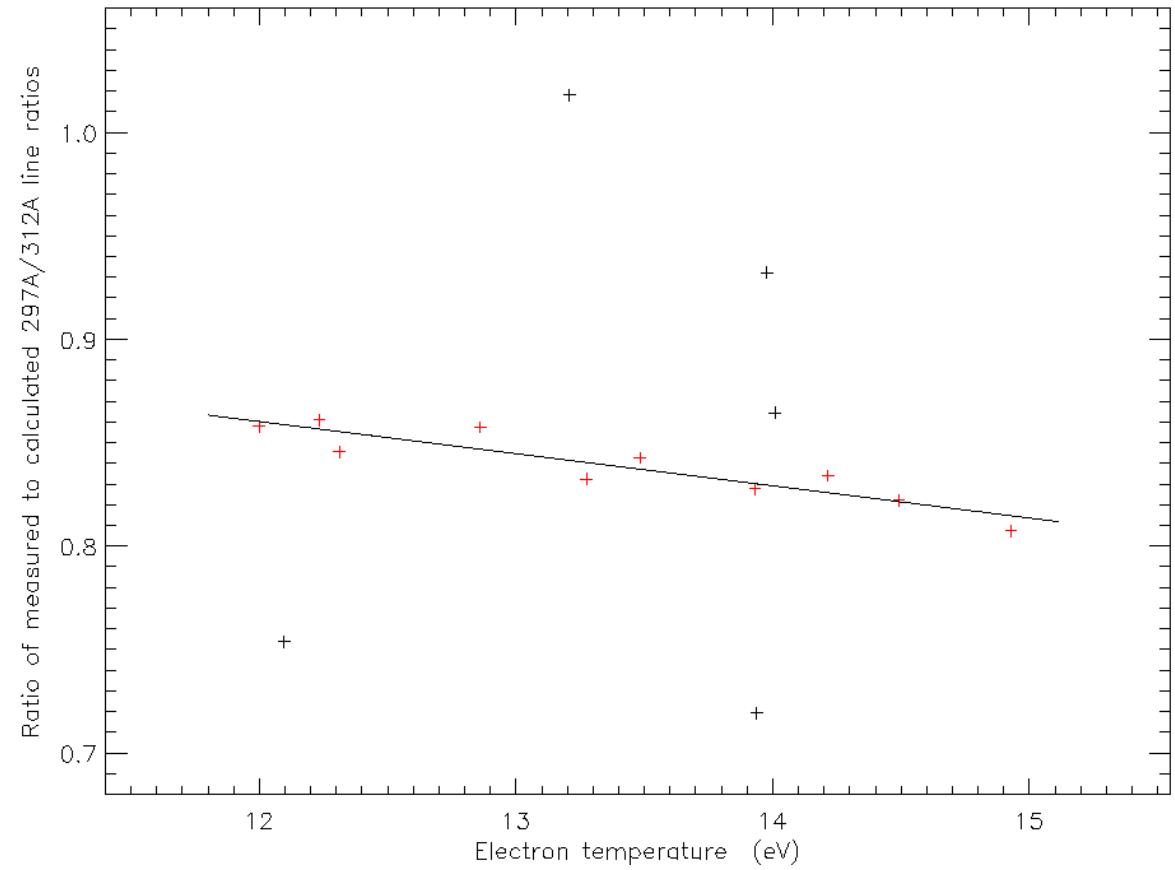

Figure 15.

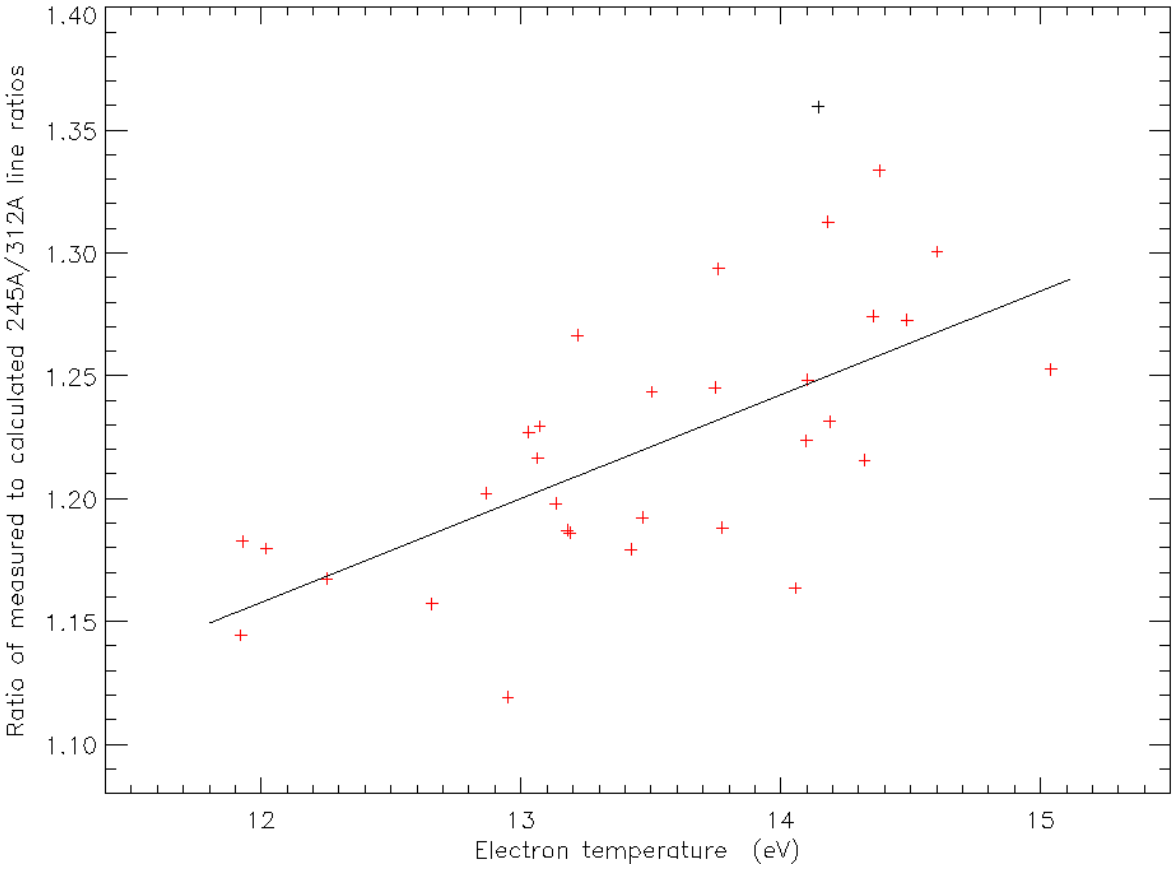

Figure 16.

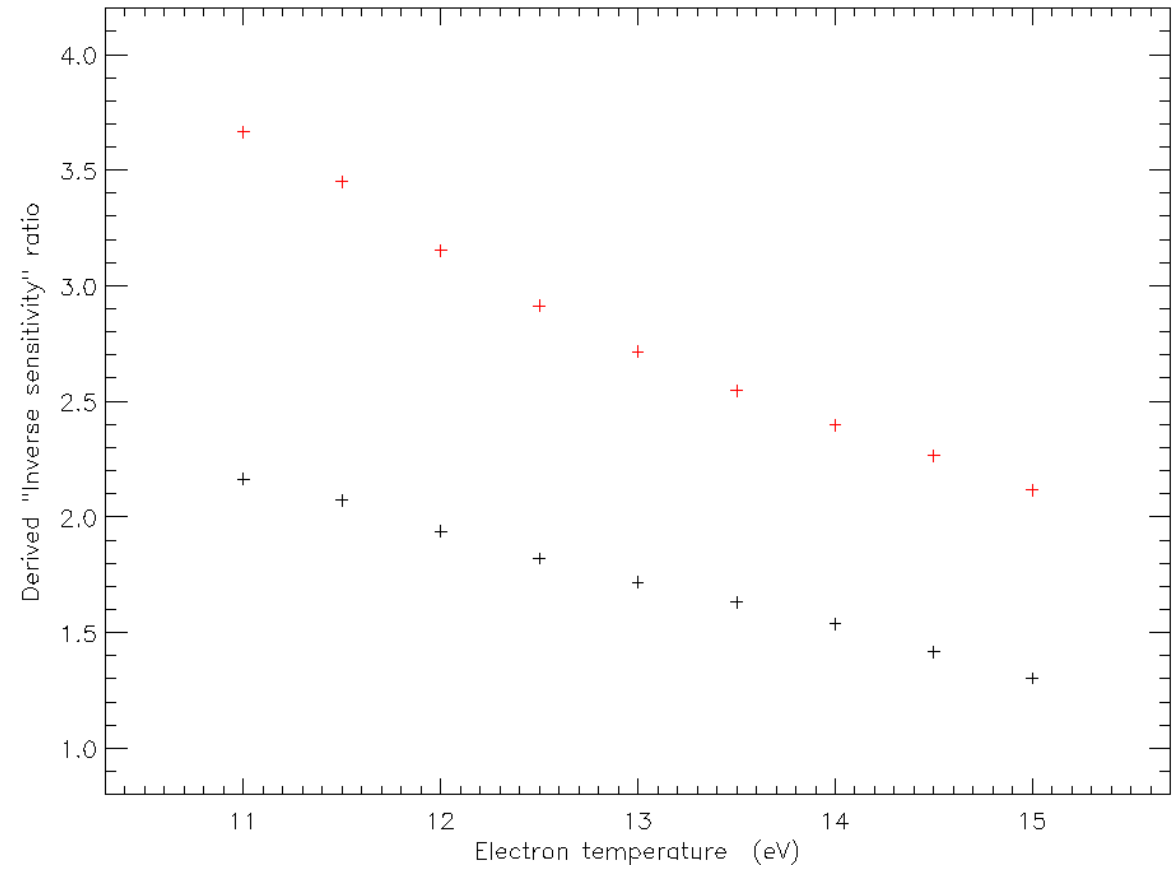

Figure 17.